037098

ADA020092

# CO₂ LASER

W. [illegible] and R.E. Center

## FINAL TECHNICAL REPORT

Contract No. N00014-72-C-0030
January 1976

sponsored by

ADVANCED RESEARCH PROJECTS AGENCY
ARPA Order No. 1807

Reproduced by
NATIONAL TECHNICAL
INFORMATION SERVICE
US Department of Commerce
Springfield, VA. 22151

PRICES SUBJECT TO CHANGE

AVCO EVERETT RESEARCH LABORATORY, INC.
A SUBSIDIARY OF AVCO CORPORATION

BEST
AVAILABLE COPY

U.S. DEPARTMENT OF COMMERCE
National Technical Information Service
AD-A020 092

# CO LASER

AVCO EVERETT RESEARCH LABORATORY, INCORPORATED

PREPARED FOR
OFFICE OF NAVAL RESEARCH

30 JUNE 1975

# KEEP UP TO DATE

Between the time you ordered this report—which is only one of the hundreds of thousands in the NTIS information collection available to you—and the time you are reading this message, several *new* reports relevant to your interests probably have entered the collection.

Subscribe to the **Weekly Government Abstracts** series that will bring you summaries of new reports *as soon as they are received by NTIS* from the originators of the research. The WGA's are an NTIS weekly newsletter service covering the most recent research findings in 25 areas of industrial, technological, and sociological interest—invaluable information for executives and professionals who must keep up to date.

The executive and professional information service provided by NTIS in the **Weekly Government Abstracts** newsletters will give you thorough and comprehensive coverage of government-conducted or sponsored research activities. And you'll get this important information within two weeks of the time it's released by originating agencies.

WGA newsletters are computer produced and electronically photocomposed to slash the time gap between the release of a report and its availability. You can learn about technical innovations immediately—and use them in the most meaningful and productive ways possible for your organization. Please request NTIS-PR-205/PCW for more information.

The weekly newsletter series will keep you current. But *learn what you have missed in the past* by ordering a computer **NTISearch** of all the research reports in your area of interest, dating as far back as 1964, if you wish. Please request NTIS-PR-186/PCN for more information.

WRITE: Managing Editor
5285 Port Royal Road
Springfield, VA 22161

# Keep Up To Date With SRIM

SRIM (Selected Research in Microfiche) provides you with regular, automatic distribution of the complete texts of NTIS research reports *only* in the subject areas you select. SRIM covers almost all Government research reports by subject area and/or the originating Federal or local government agency. You may subscribe by any category or subcategory of our WGA **(Weekly Government Abstracts)** or **Government Reports Announcements and Index** categories, or to the reports issued by a particular agency such as the Department of Defense, Federal Energy Administration, or Environmental Protection Agency. Other options that will give you greater selectivity are available on request.

The cost of SRIM service is only 45¢ domestic (60¢ foreign) for each complete microfiched report. Your SRIM service begins as soon as your order is received and processed and you will receive biweekly shipments thereafter. If you wish, your service will be backdated to furnish you microfiche of reports issued earlier.

Because of contractual arrangements with several Special Technology Groups, not all NTIS reports are distributed in the SRIM program. You will receive a notice in your microfiche shipments identifying the exceptionally priced reports not available through SRIM.

A deposit account with NTIS is required before this service can be initiated. If you have specific questions concerning this service, please call (703) 451-1558, or write NTIS, attention SRIM Product Manager.

This information product distributed by

NTIS U.S. DEPARTMENT OF COMMERCE
National Technical Information Service
5285 Port Royal Road
Springfield, Virginia 22161

UNCLASSIFIED

SECURITY CLASSIFICATION OF THIS PAGE (When Data Entered)

| REPORT DOCUMENTATION PAGE | | READ INSTRUCTIONS BEFORE COMPLETING FORM |
|---|---|---|
| 1. REPORT NUMBER | 2. GOVT ACCESSION NO. | 3. RECIPIENT'S CATALOG NUMBER |
| 4. TITLE (and Subtitle)<br>CO Laser | | 5. TYPE OF REPORT & PERIOD COVERED<br>Final Technical Report<br>11/1/71 to 6/30/75 |
| | | 6. PERFORMING ORG. REPORT NUMBER |
| 7. AUTHOR(s)<br>M. J. W. Boness and R. E. Center | | 8. CONTRACT OR GRANT NUMBER(s)<br>N00014-72-C-0030 |
| 9. PERFORMING ORGANIZATION NAME AND ADDRESS<br>Avco Everett Research Laboratory, Inc.<br>2385 Revere Beach Parkway<br>Everett, MA 02149 | | 10. PROGRAM ELEMENT, PROJECT, TASK AREA & WORK UNIT NUMBERS<br>Code No. 421 |
| 11. CONTROLLING OFFICE NAME AND ADDRESS<br>Advanced Research Projects Agency<br>Department of Defense<br>ARPA Order No. 1807 | | 12. REPORT DATE<br>January, 1976<br>13. NUMBER OF PAGES<br>71 |
| 14. MONITORING AGENCY NAME & ADDRESS (if different from Controlling Office)<br>Office of Naval Research<br>Arlington, Virginia 22217 | | 15. SECURITY CLASS. (of this report)<br>Unclassified<br>15a. DECLASSIFICATION/DOWNGRADING SCHEDULE |

16. DISTRIBUTION STATEMENT (of this Report)

Approved for public release; distribution unlimited.

17. DISTRIBUTION STATEMENT (of the abstract entered in Block 20, if different from Report)

18. SUPPLEMENTARY NOTES

19. KEY WORDS (Continue on reverse side if necessary and identify by block number)

Carbon Monoxide Laser
5 Microns
Cryogenic Temperature
Partial Inversion
Electron Beam Sustained Discharge
Modeling Calculations
Small Signal Gain
Medium Homogeneity
Diffraction Limited Performance

20. ABSTRACT (Continue on reverse side if necessary and identify by block number)

This report reviews and completes the present Avco Everett Research Laboratory high-pressure, pulsed CO laser program. The main program objective has been the investigation of the pulsed electrical CO laser to determine the relevant scaling parameters and usefulness of high-power CO lasers in systems applications. Detailed description of the earlier work performed mainly on the 20 liter device is contained in previous reports. These include measurements of parametric multiline/multimode performance, medium homogeneity investigations and measurements of small signal gain.

DD FORM 1 JAN 73 1473 EDITION OF 1 NOV 65 IS OBSOLETE

UNCLASSIFIED

SECURITY CLASSIFICATION OF THIS PAGE (When Data Entered)

A detailed kinetic model of the CO laser was developed and the predictions compared with the experimental results. Results of similar measurements performed on the new 16 liter transverse flow device are presented. Major achievements included operation at high power, high efficiency and with near-diffraction-limited beam quality.

## FOREWORD

| | |
|---|---|
| ARPA Order No: | 1807 |
| Program Code No: | 421 |
| Contract No: | N00014-72-C-0030 |
| Principal Investigator and Phone No: | 617-389-3000, Ext. 451 |
| Name of Contractor: | AERL, Inc. |
| Effective Date of Contract: | 11-1-71 |
| Contract Expiration Date: | 6-30-75 |
| Amount of Contract: | $884,079 |
| Scientific Officer: | Director, Physics Program,<br>Physical Sciences Division,<br>Office of Naval Research,<br>Department of the Navy,<br>800 No. Quincy Street,<br>Arlington, VA 22217 |
| Short Title of Work: | CO Laser |

## ABSTRACT

This report reviews and completes the present Avco Everett Research Laboratory high-pressure, pulsed CO laser program. The main program objective has been the investigation of the pulsed electrical CO laser to determine the relevant scaling parameters and usefulness of high-power CO lasers in systems applications. Detailed description of the earlier work performed mainly on the 20 liter device is contained in previous reports. These include measurements of parametric multiline/multimode performance, medium homogeneity investigations and measurements of small signal gain. A detailed kinetic model of the CO laser was developed and the predictions compared with the experimental results. Results of similar measurements performed on the new 16 liter transverse flow device are presented. Major achievements included operation at high power, high efficiency and with near-diffraction-limited beam quality.



Preceding page blank

TABLE OF CONTENTS





Preceding page blank

## LIST OF ILLUSTRATIONS





Preceding page blank

## LIST OF TABLES

# 1.0 INTRODUCTION

The overall objective of this combined experimental and theoretical program was to investigate the fundamental physics of the high pressure electrical CO laser and, thereby, to develop the technology for high pressure, scalable, electric CO lasers exhibiting properties of high electrical efficiency, good beam quality and with the potential for repetitively pulsed operation. The specific achievements of this three and a half year program include: 1) the development of a detailed kinetic model of the pulsed electric CO laser to model the laser performance as well as to obtain predictions of operating performance under a variety of experimental conditions; 2) the measurement of the electron-ion recombination rate in high pressure CO discharges; 3) the development of the technology for pulsed CO lasers operating with cryogenic gas temperatures in room temperature surroundings with good medium homogeneity to produce near diffraction limited beam quality; 4) parametric measurements of the performance of the high pressure, large volume, scalable electric CO laser including measurements of efficiency, specific energy, spectral distribution, small signal gain behavior and beam quality.

The development of the kinetic model of the pulsed electrical CO laser, was based on a previous theoretical investigation[1, 2] of the effects of anharmonicity on the vibrational distribution in a diatomic molecule under conditions of thermal nonequilibrium. The detailed kinetic model was developed to predict the time dependence of the total lasing efficiency, spectral distribution of the stimulated transitions, energy partitioning in the vibrational and translational modes, and translational temperature history in various CO-$N_2$ and CO-Ar mixtures. The numerical results have been compared with specific experimental measurements of pulse electrical efficiency, spectral distribution, and small signal gain variations. Although the model predictions are in overall agreement with the temporal variation of the laser pulse and the parametric dependence of efficiency, onset delay times with gas mixture, there are several significant discrepancies between the model calculations and the measurements, specifically, the maximum small signal gain and the temporal variation of the small signal gain. This is discussed in detail in Sections II and V. Section II also includes reference to some earlier measurements of electron-ion recombination rate constants in high pressure discharges in CO-$N_2$ gas mixtures. These measurements indicated large rate coefficients for the recombination process thereby implying that electric discharges in CO lasers should be dominated by electron-ion recombination rather than attachment processes.

Two different room temperature discharge cavities were designed and built under this program for operation with cryogenic gases together with the necessary electron beam source and sustaining discharge power supplies.

The first discharge cavity had a nominal excitation volume of 20 liters and was used for experimental measurements at both room temperature and cryogenic inlet temperatures. Table I summarizes the maximum pulse energies and efficiencies at the two different operating temperatures in this device. The efficiency is defined as the ratio of the measured lasing output energy to the entire energy deposited into the discharge, as determined from the discharge current and voltage waveforms. No corrections have been applied either for window losses or for the fact that the electrical energy is deposited over a larger volume than that defined by the stable resonator. Interferometric measurements of the medium quality in this device indicated very large thermal nonuniformities due to buoyancy forces which dominated inertia forces because of the very low flow velocities involved (of the order of 10 cm per sec). This was confirmed by some measurements with an unstable resonator which yielded highly nonuniform distribution of flux in the laser beam. [3]

In order to overcome the thermal nonuniformities observed in the first discharge cavity, a second cavity system was designed with transverse flow through the discharge, typical flow velocities being of the order of 300 cm per sec. This system had an active volume of approximately 16 liters. A cryogenic heat exchanger was developed[3] for use with the second cavity, the overall objective being to demonstrate excellent thermal uniformity in the system while maintaining a large temperature difference between the gas and the walls thereby allowing operation with a room temperature environment. Some performance characteristics of the second discharge cavity are listed in Table II. Near field burn patterns with this device indicated 1.5 x near-diffraction limited beam quality in agreement with the interferometric measurements both with and without power loading in the discharge.

Experimental results of beam quality, pulse energy and efficiency, spectral distribution and small signal gain are described in Section V. Small signal gain measurements were made in both discharge cavities and the results exhibited several significant discrepancies with the theoretical model predictions. These discrepancies include lack of evidence of absorption before gain build-up in the high vibrational transitions and a factor of 2 - 4 disagreement in the magnitude of the peak small signal gain. These discrepancies have not yet been satisfactorily explained and are discussed in Section V. Another interesting result of the small signal gain measurements was the first experimental observation of resonance self-absorption by overlapping transitions under high pressure/density operations. This mechanism is responsible for gain suppression on certain transitions.

Much of the work in this program has been described in previous contractual reports except for the performance characteristics of the new transverse flow discharge cavity. Only brief details of this earlier work in the 20 liter discharge system are included in this final report and the references are listed at the end of the report. However, an attempt has been made to summarize the pertinent results and detailed description is given of recent experimental results with the new discharge cavity.

TABI E I

PERFORMANCE CHARACTERISTICS OF 20 LITER DISCHARGE CAVITY

Mixture ratio 20% CO: 80% Diluent

Density ~ 1/3 amagat

| Temperature* (°C) | Diluent | Sustainer Electric Field (kV/cm) | Laser Output (joules) | Discharge Pulse Length ($\mu$secs) | Efficiency** (%) |
|---|---|---|---|---|---|
| -140 | $N_2$ | 2.5 | 1500 | 90 | 20 |
| | Ar | 1.3 | 1700 | 90 | 19 |
| 20 | $N_2$ | 3.0 | 700 | 80 | 6 |
| | Ar | 2.0 | 200 | 40 | 4 |

*Estimated minimum temperature based on interferometry and thermocouple measurements.

**The Efficiency is defined as the ratio of the measured lasing output energy to the entire energy deposited into the discharge, as determined from the discharge current and voltage waveforms.

TABLE II

PERFORMANCE CHARACTERISTICS OF 16 LITER TRANSVERSE FLOW CAVITY

Mixture ratio 20% CO: 80% Diluent

Density ~ 1/2 amagat

Temperature 80°K to 100°K

Beam quality better than 1.5 X diffraction limited

| Diluent | Sustainer Electric Field | Laser Output* | Discharge Pulse Length | Efficiency |
|---|---|---|---|---|
| | (kV/cm) | (joules) | (μsecs) | (%) |
| $N_2$ | 2.5 | 1560 | 60 | 35 |
| Ar | 1.1 | 1010 | 40 | 38 |

*Output corrected for loss due to one uncoated window

# 2.0 KINETICS

## 2.1 MODELING

The basic physics describing the kinetic processes appropriate to the electrically excited CO laser are contained in the master vibrational rate equations for the density of molecules in each vibrational level. These equations have been reported elsewhere and are outlined in Appendix A together with the appropriate gain and output flux equation. Since the collisional relaxation processes and the gain are dependent on the translational temperature its variation was computed by consideration of all processes in which energy is transferred to the translational degree of freedom. An independent check on this temperature calculation was obtained by an overall energy balance at each time interval in the computation.

In the analysis the rotational temperature is taken to be in equilibrium with the kinetic/translational temperature since the time scale for rotational relaxation is expected to be several orders of magnitude faster than any other collisional[3] or radiative process. Furthermore, the calculations are restricted to only one vibration/rotation line which can oscillate between each pair of vibrational levels and the rotational transition chosen is that corresponding to the maximum gain for that pair of vibrational levels. The optical cavity is assumed to be formed by two parallel mirrors with output coupling, $L_c$, and separated by a length, $\ell$. Axial variations in the cavity flux have been neglected since it can be readily shown [4] that this variation is less than 10% for an output coupling of 60% or less.

The general form of the electron impact excitation is determined by the electron density, $N_e$, and the rate constants, $k_e^{i,v}$, for electron impact excitation from vibrational level i to level v. This rate constant requires detailed knowledge of the electron kinetics. For a uniform discharge with a constant ratio of electric field to gas density, E/N, the Boltzmann equation is solved[5, 6] for the non-Maxwellian electron velocity distribution function. This distribution function is then integrated over the vibrational excitation cross section data to obtain the excitation rate constants. The electron impact vibrational excitation cross sections for CO and $N_2$ have been measured[7-9] for excitation from the zeroth to the first ten excited vibrational levels. There is, as yet, no experimental data on the excitation cross sections from one excited vibrational level to another level in CO or $N_2$.

The Boltzmann equation was solved including vibrational excitation from the zeroth vibrational level to the first eight vibrational levels. For the range of E/N of interest here, typically less than $3 \times 10^{-16}$ volt-cm$^2$, the excitation above the eighth level can be neglected being less than 0.1% of the total vibrational excitation. Since the kinetic calculations predict a

significant population growth in the excited levels, typically 30% of the CO molecules, some allowance must be made for excitation from these levels. In the absence of experimental cross section data from excited levels it has been assumed that the net excitation rate remains unchanged as the vibrational distribution is altered. This implies that the excitation rate constants are treated to be primarily a function of energy loss and quite insensitive to the initial vibrational state of the molecule. One of the pitfalls in this assumption is that vibrationally excited levels of CO lie closer energetically to the resonance state of $CO^-$ which provides the dominant contribution to the excitation cross sections and therefore the energy dependences for further excitation from these levels will shift towards lower energies as the initially excited level more closely approaches the resonance. This will clearly alter the overlap of the cross section and the electron energy distribution and may invalidate the assumption that the rate constants be treated as suggested. The situation is complicated by the fact that the overall shape of the cross sections from excited states may not be constant for constant energy loss and until accurate calculations or reliable measurements of the relevant cross sections become available the actual values of the rate constants will remain in doubt.

Proceeding however on the assumption that the rate constants be treated only as function of energy loss leads to a fixed net vibrational excitation rate, i.e. rate of total vibrational excitation, but with a modified distribution to each level[6] depending on the initial vibrational distribution. One other approximation has been made in obtaining the Boltzmann solution to the electron velocity distribution function in that collisions of the second kind were neglected.

It is expected that these approximations will lead to errors in the detailed distribution of excitation rate constants however if these changes do not affect the rate of total vibrational excitation then they are not expected to have a major impact on the present numerical calculations for high pressure electrical lasers. This conclusion follows from considerations of the operating conditions in the electron beam sustained discharges. The pressure is typically of the order of one atmosphere so that the characteristic time for vibration-vibration relaxation, $\tau_{V-V}$, is of the order of $10^{-6}$ to $10^{-7}$ secs. This is much less than the corresponding time scale for single quantum vibrational excitation which is of the order of $10^{-4}$ to $10^{-5}$ secs for typical electron densities of $10^{13}$ per $cm^3$ or less. Under these conditions the overall heavy particle kinetics should be insensitive to perturbations in the distribution of excitation rate constants. Thus, the calculations are quasi cw in the sense that the vibrational distribution reaches a local equilibrium on a time scale short compared with the rate of electrical energy input. These calculations are therefore also appropriate to cw excitation such as in existing supersonic CO lasers.[10] It should be pointed out that the present approximations break down if the ratio of electron density to CO density is increased by an order of magnitude or more. Thus, the present calculations would not be applicable to the high electron density, short pulse calculations of Rockwood, et al.[11] Furthermore it is unlikely that the detailed modifications to the various rate constants derived from

properly including the effects of excited states would conspire to validate the simple assumptions regarding their role in affecting the electron kinetics and more refined calculations are clearly desirable.

## 2.2 ELECTRON-ION DISSOCIATIVE RECOMBINATION RATE CONSTANT

Prior to this program there were no data available on the dominant electron loss processes in high density discharges in CO. Since these loss processes determine the required electron beam source strength some measurements were made of the effective electron-ion recombination rate constant with CO densities up to 1 amagat and electron temperatures varying from 0.2 to 0.7 eV, the ion and neutral temperatures being approximately 300°K.

The measurements are fully described in an earlier publication[12] and only the major conclusions are presented here:

1) The dominant electron loss mechanism is two body dissociative recombination, the principal ion at the high experimental densities probably being the polymer[13] $CO^+.(CO)_n$ where $n \leq 3$

2) The effective two-body rate coefficient was found to be in the range $10^{-7}$ - $10^{-6}$ $cm^3/sec$, with an electron temperature dependence of $Te^{-1.6}$ associated with the average electron energy from 0.2 to 0.7 eV.

3) A weak pressure dependence, of less than a factor of 2, was observed as shown in Fig. 1 which summarizes the results.

## 2.3 COMPARISON OF MODEL PREDICTIONS WITH EXPERIMENTAL DATA

The kinetic model has been used to develop detailed predictions of the pulse energy, temporal variation, small signal gain and spectral distribution for comparison with experimental data obtained in this program. These comparison are presented in Section V as well as being described in previous reports. The present discussion is therefore limited to the major agreement and discrepancies between the model and the experimental data.

The general pulsed characteristics and predicted parametric variation with mixtures are in reasonable agreement with the experimental results; an example is shown in Figs. 2 and 3 for the comparison between the experimental and predicted temporal variation of the output pulse, using $N_2$ and Ar as diluents respectively. These predictions are relatively insensitive to the detailed kinetic input data such as the V-V relaxation rates for reasons described above, namely that the vibrational distribution reaches a local equilibrium on a time scale short compared with the rate of electrical energy input. The variation of the total efficiency and the delay time to reach threshold with the gas mixture[14] in $CO-N_2$ experiments are in qualitative agreement with the model predictions.

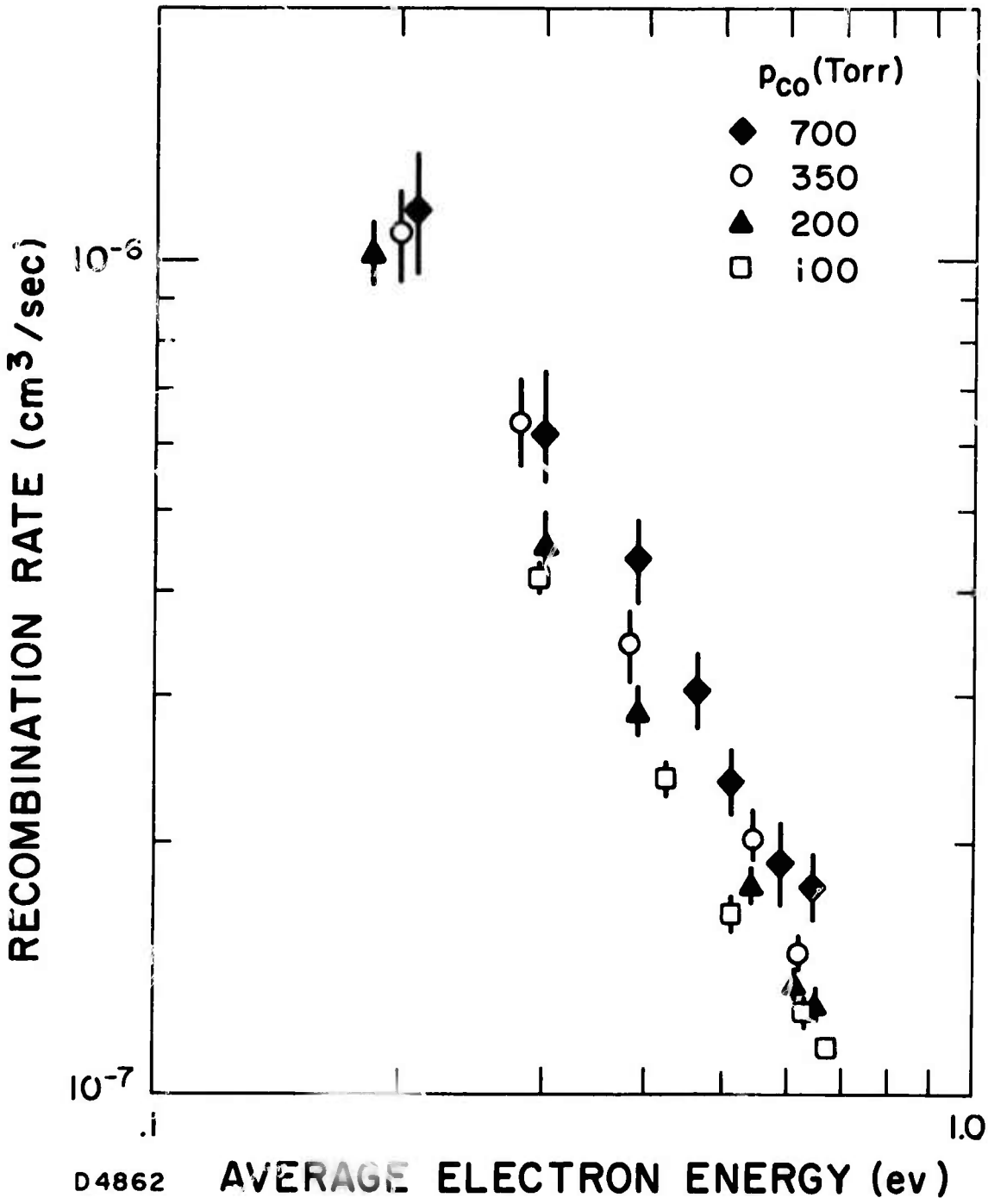


Fig. 1 Plot of Electron-Ion Recombination Rate in Pure CO as a Function of Average Electron Energy

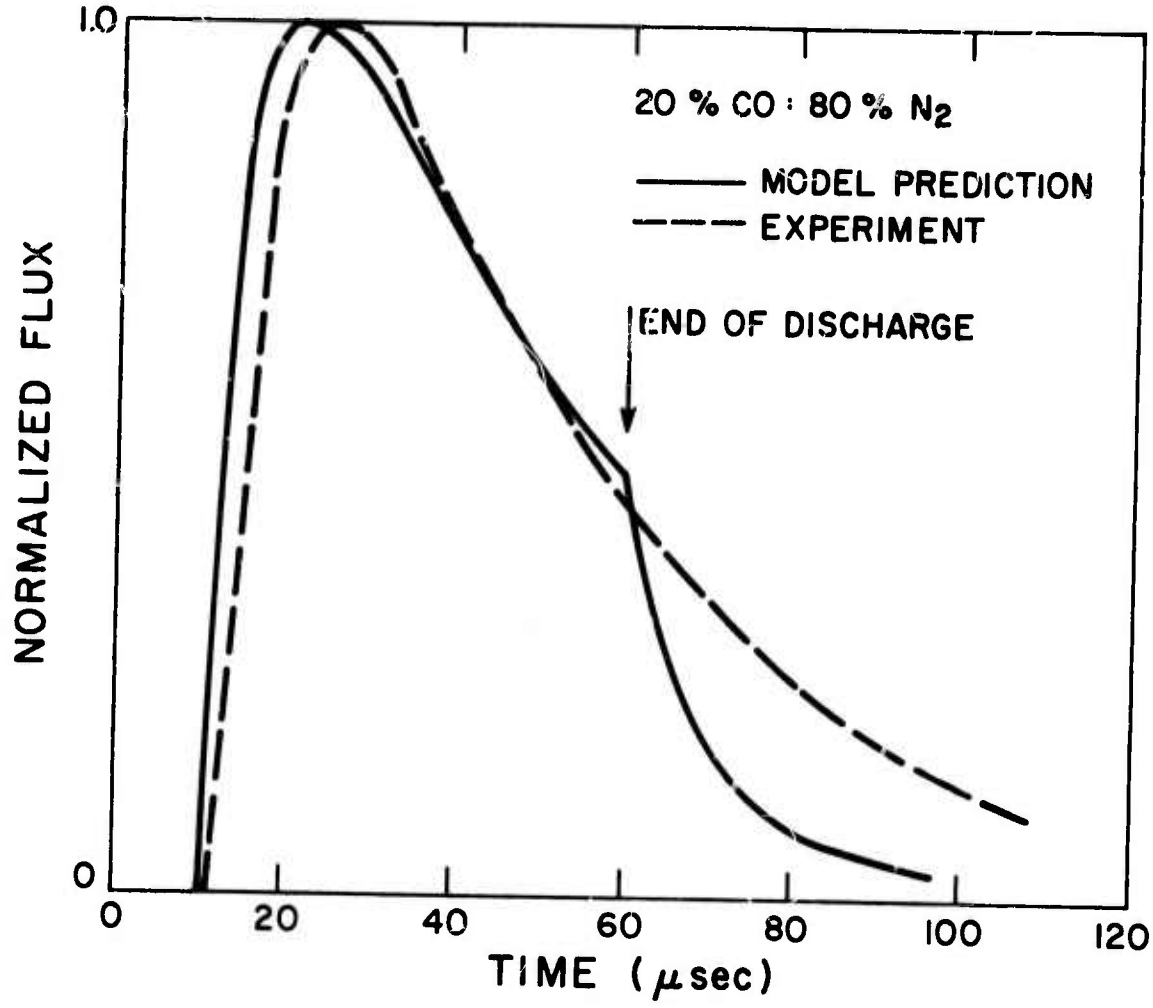


Fig. 2 Comparison of the Normalized Experimental and Predicted Temporal Behavior of the Laser Output Pulse for a 20% CO and 80% $N_2$ Mixture

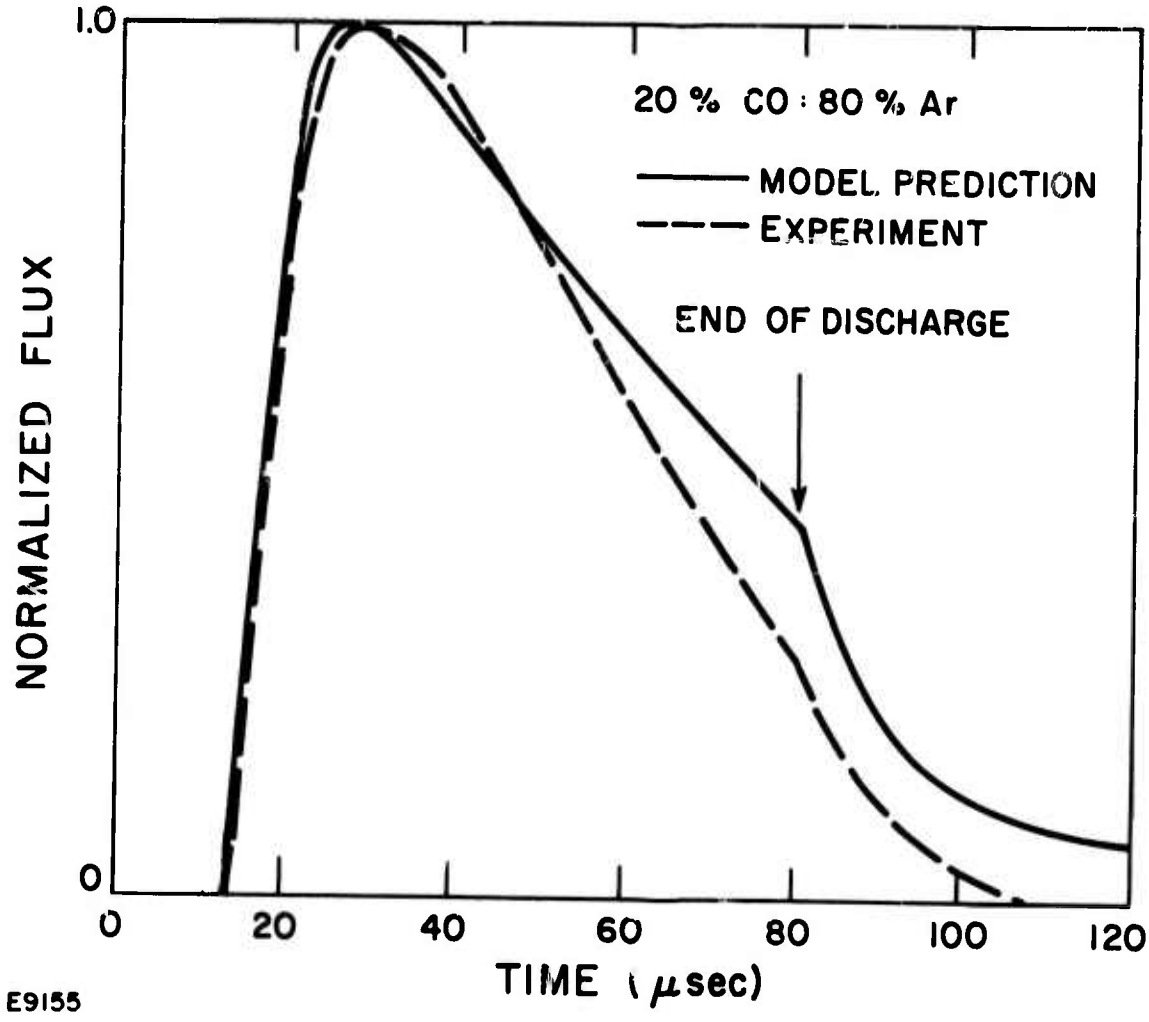


Fig. 3 Comparison of the Normalized Experimental and Predicted Temporal Behavior of the Laser Output Pulse for a 20% CO and 80% Ar Mixture

Although the model predicts consistently higher efficiencies than experimentally observed, even with the very uniform 16 liter discharge cavity, the discrepancy may well be due to parasitic oscillations as described in Section V. The maximum experimental efficiencies observed in this program were approximately 35% as compared with the predicted 50 to 60% overall electrical efficiency. It should be pointed out that similar experimental measurements at Northrop have indicated higher efficiencies up to 60% in reasonable agreement with the kinetic model.

While the general predictions of the kinetic model are in fair agreement with the experimental data, some of the detailed predictions are in strong disagreement, an example of this being the predictions for the temporal variation of small signal gain[15]. In particular, the predicted maximum small signal gain is always found to be a factor of 2 to 4 larger than the experimentally observed gain. Furthermore, the model calculations predict that in the approach to the quasi steady vibrational distribution the partial inversion on any vibrational level should be preceded by absorption as energy flows up the vibrational ladder. Figure 4 shows an example of the predictions for the small signal gain behavior for the P12 line of various vibrational levels. These calculations illustrate the time variation of the flow of energy up the vibrational ladder and indicate absorption ahead of gain which was not observed experimentally. Experimental measurements in both discharge cavities failed to observe this absorption characteristic and this implies either a fundamental error in the kinetic model or an error in the kinetic data used in the model. The latter hypothesis may well be true since the detailed vibrational distribution predicted by the model and the resultant small signal gain behavior are sensitively dependent upon the kinetic data such as the vibrational relaxation rate constants for a multitude of vibrational interactions as well as the detailed electron excitation kinetics.

In view of this discrepancy between the calculated and observed temporal gain dependence, further kinetics calculations were performed substituting variously increased relaxation rates for both the near and nonresonant collisions. This procedure reduced the amplitude of the predicted absorption but never suppressed it entirely. However, there is no justification for this procedure since the rates originally employed[1] agree well with the limited available experimental data.[16] It should be pointed out here that in general the probabilities for V-V and V-T relaxation processes have only been measured experimentally for the low vibrational levels of CO and various theoretical models[1] have been applied to predict the high level relaxation probabilities normalized to the experimental value for the low levels. The electron kinetics have been less rigorously treated due, principally, to the lack of available experimental data describing collisions with vibrationally excited molecules and furthermore collisions of the second kine were not included.

These results and the discrepancy with the experiments indicate the need for more detailed electron & molecular kinetic data as well as further investigation of the underlying physics in the kinetic model in order

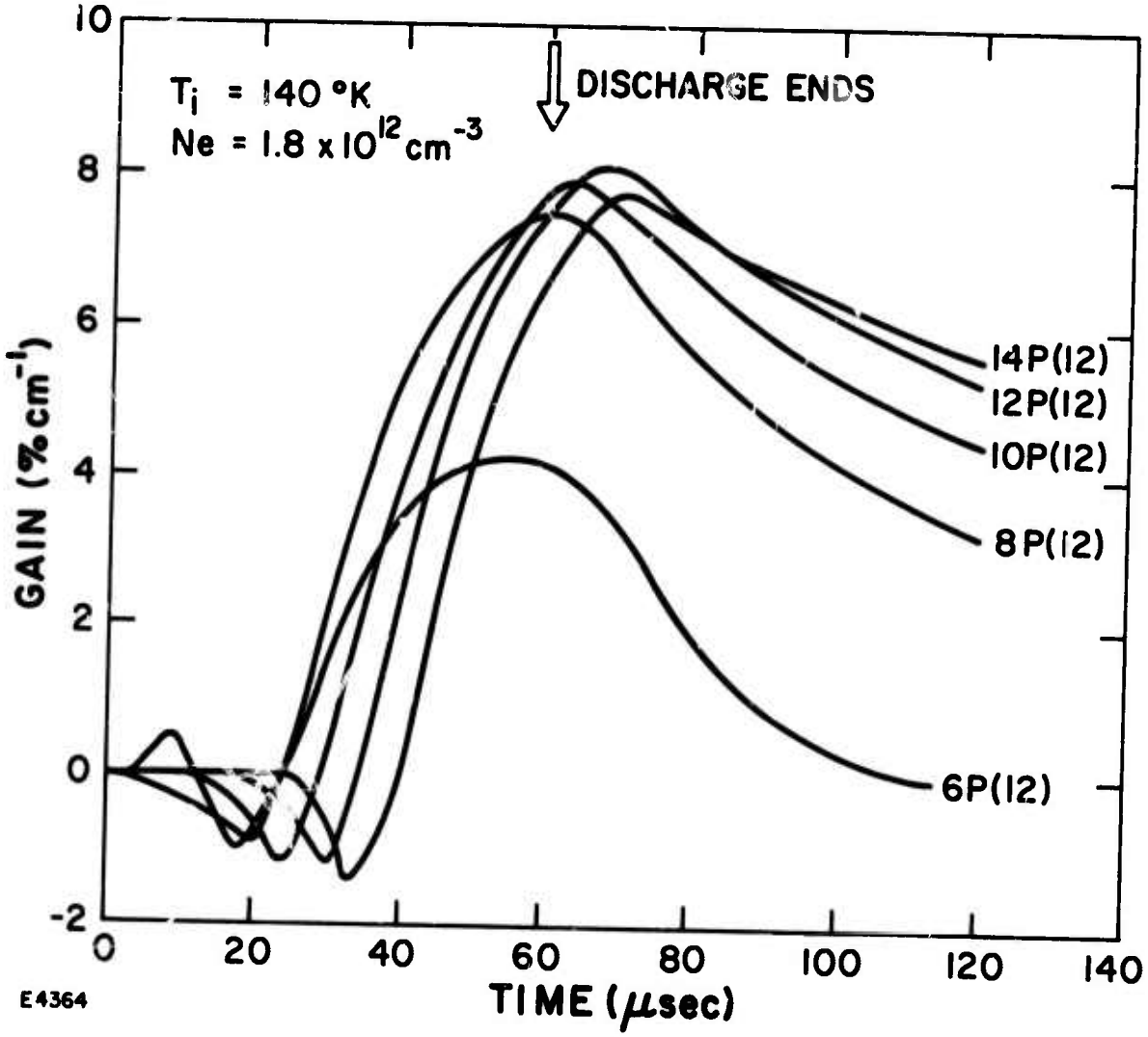


Fig. 4 Predictions of the Temporal Variation of Small-Signal Gain for the P (12) Line of Various Vibrational Bands

to improve the agreement with experiment and the understanding of the CO laser. It should be re-emphasized however that the significant discrepancy between theory and experiment is only evident in detailed measurements directly related to the development of the vibrational distribution function and the more general laser character predictions appear to be in reasonable agreement with the data.

## 3.0 DISCHARGE CAVITY/FLOW SYSTEM

One of the primary aims of this program has been the development of room temperature discharge cavities capable of operating with cryogenic gas flow, and at the same time maintaining good density uniformity in the gas. The intent here is to avoid materials compatibility problems due to differential contraction and expansion of the hardware and electron beam interface which would occur if the discharge cavity were completely cooled to cryogenic temperatures. An even greater problem at cryogenic temperatures concerns the interface with the window material, $CaF_2$ being the usual material for 5 $\mu$ systems. Any room temperature design system clearly has practical advantages over a cryogenically cooled system, not least of which is the necessity in a cryogenically cooled system to maintain vacuum insulation surrounding the system. In the initial phase of the program a 20 liter discharge cavity system was designed and built with cryogenically cooled electrodes and gas supply but room temperature walls. This system, shown schematically in Figs. 5 and 6, has been described in several previous reports[17-19] and was used for all the initial performance measurements. Because of the small flow velocity in this system (10-20 cm/sec) buoyancy forces lead to considerable thermal nonuniformities[1], which severely limited the performance of the device and in particular the optical beam quality.

As a result of the experience gained with this initial 20 liter discharge cavity, a new transverse gas flow system was designed and built to overcome the thermal nonuniformities. A schematic of the flow system is shown in Fig. 7. The basic concept of the new system was to introduce the gas through a porous heat exchanger and allow free convection boundary layers to be established on the room temperature side and end walls. The flow was directed vertically upwards to insure that buoyancy effects were favorable and to avoid recirculation. The system was designed to produce a uniform flow entering the cavity and thereby allow formation of controlled boundary layers on the side and end walls. Boundary layers (as opposed to recirculation zones) are desirable because they concentrate the density change in a narrow region and isolate the main cold flow from the warm walls. In addition, the transverse flow configuration had the advantage of utilizing the smallest cross sectional area in the system thereby maximizing the flow velocity for a given pumping speed. This design clearly has potential application to repetitively pulsed operations.

The new 16 liter flow system was designed for operation over the temperature range from 80°K to 300°K, and was made to be compatible with the existing 20 cm x 100 cm electron gun. Eventually the 500 cfm Stokes pump originally employed to evacuate and to pump the flowing gas system was abandoned in favour of a dump tank facility. By using a choking orifice in the pumping line the flow velocity could be varied over the range



Preceding page blank

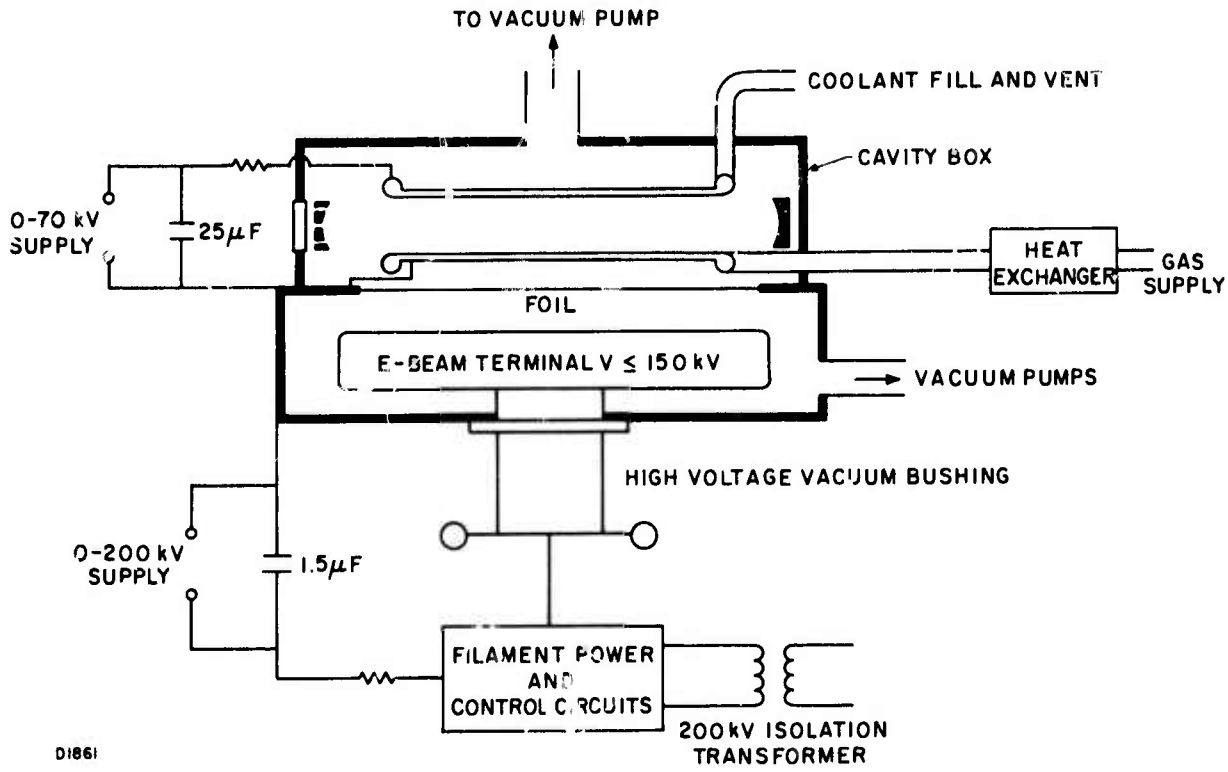


Fig. 5 Schematic of the Mk I Pulsed, High Pressure CO Laser

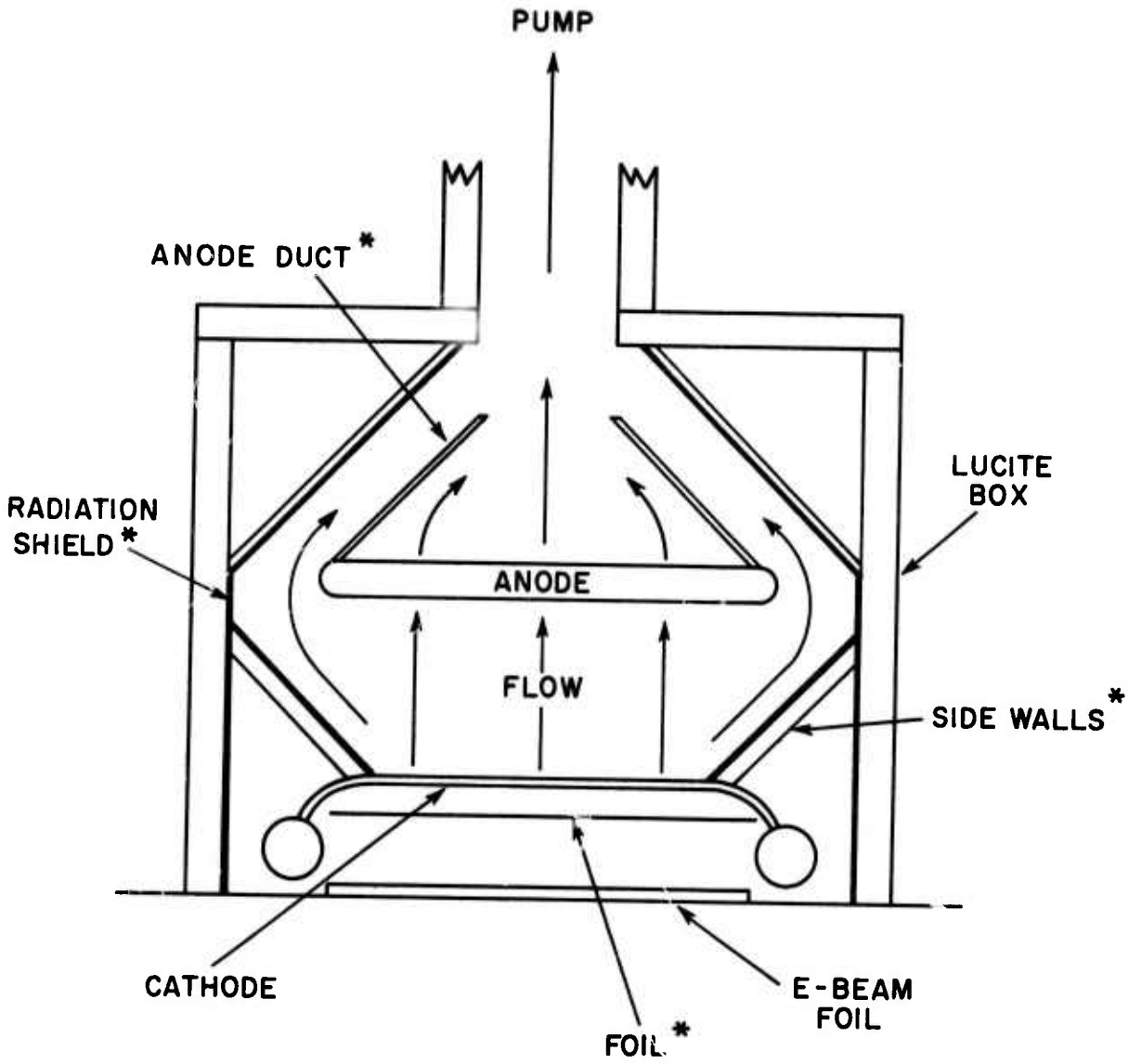


Fig. 6 Schematic of the Cross Section of the Mk I CO Laser Indicating Gas Flow and Cavity Modifications

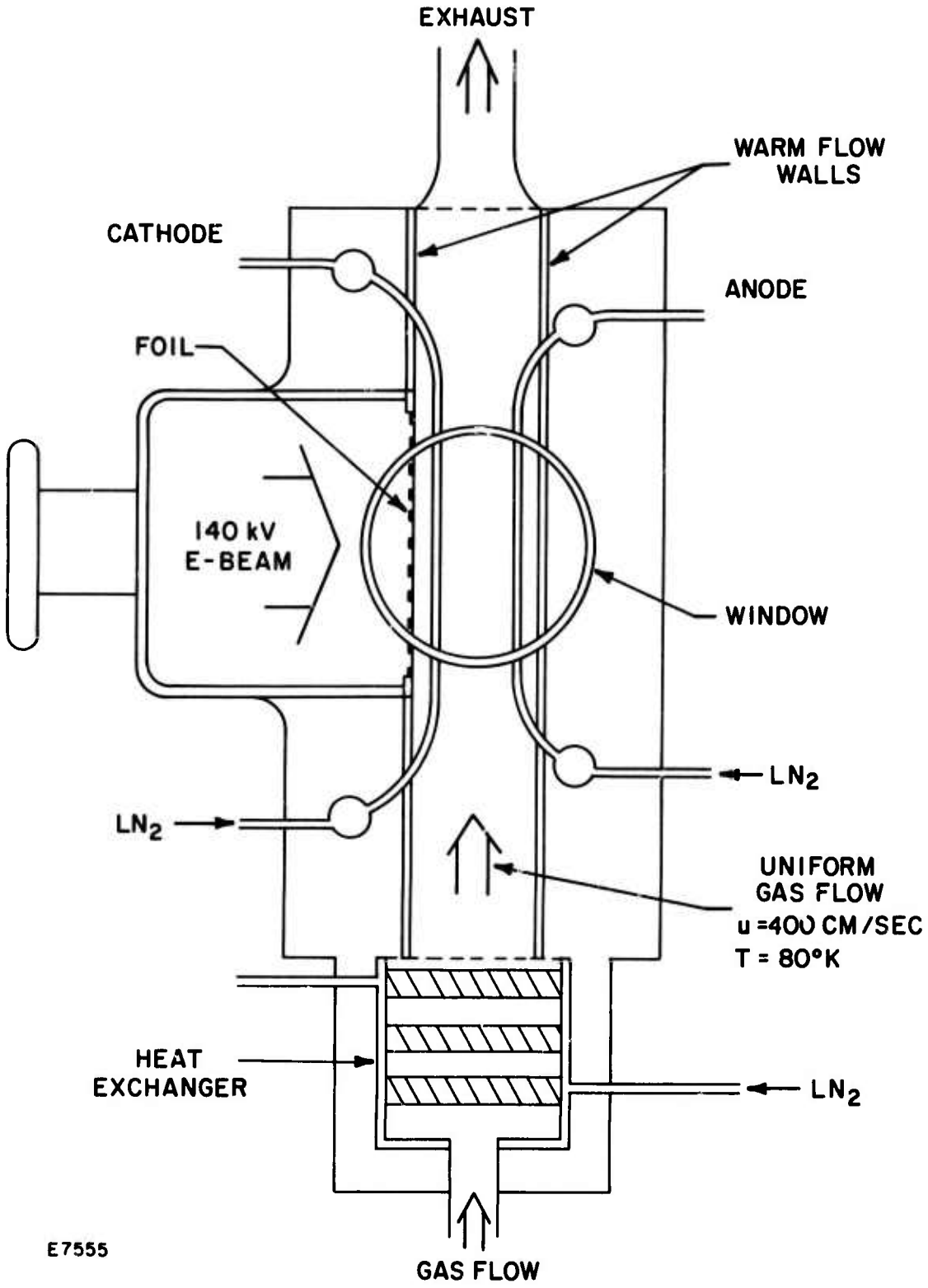


Fig. 7 Schematic of the Mk II Pulsed, High Pressure CO Laser

from 100 cm per sec to 1000 cm per sec. Boundary layer calculations indicated that medium homogeneity requirements for a near diffraction limited beam could be met with flow velocities of the order of or greater than 100 cm/sec.

The design concept of the heat exchanger was to use a pre-cooled porous plug with sufficient thermal capacity to cool the gas for transient operation of approximately 10 sec. This is more than sufficient for pulsed operation and avoids the necessity for construction of a massive heat exchanger with all its associated liquid nitrogen plumbing. The heat exchanger assembly consisted of three porous plates made of sintered bronze with liquid nitrogen tubes embedded in the porous plates. This is shown schematically in Fig. 8. A photograph of the heat exchanger showing the liquid nitrogen manifold is given in Fig. 9. The porous plates are mounted in an aluminum box which in turn is mounted inside a lucite box, (see Fig. 7). Aluminum foil radiation shielding was used around the heat exchanger and since the system is normally under vacuum, except during the pulse operation, the heat exchanger is thermally isolated from the lucite box.

The heat exchanger was instrumented with many thermocouples and cryogenic tests indicated temperature uniformity of better than 2°C (the reading accuracy on the thermocouple unit). The preliminary interferometric measurements of the medium quality, which are described in the previous semi-annual report, indicated excellent thermal uniformity in the system with an integrated temperature variation along the optical axis of a fraction of a degree C. The detailed medium uniformity tests using an interferometer with and without power loading in the gas are described in the Section IV.

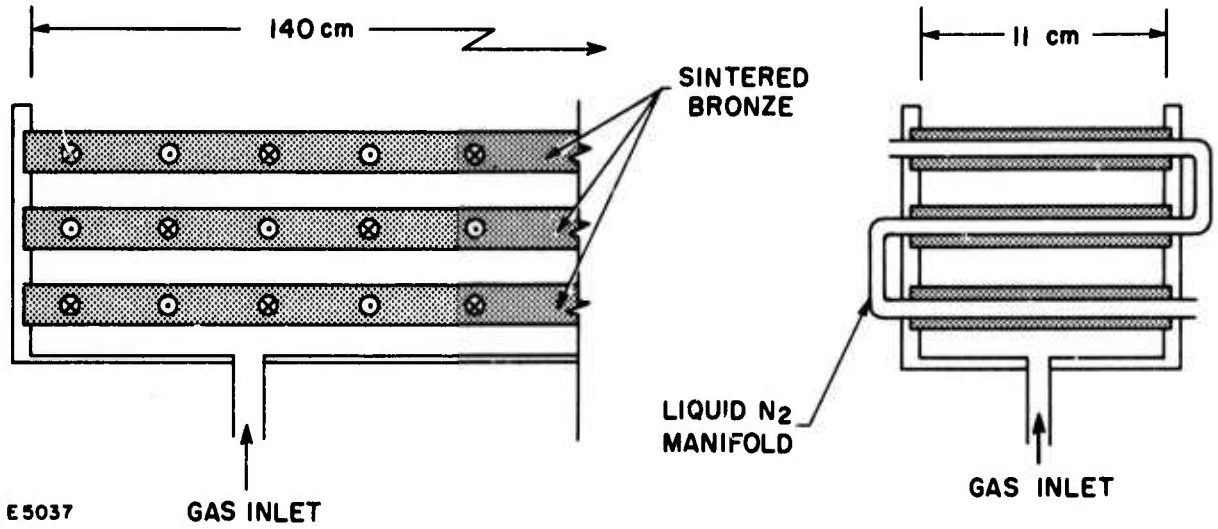


Fig. 8 Schematic of the Mk II CO Laser Heat Exchanger

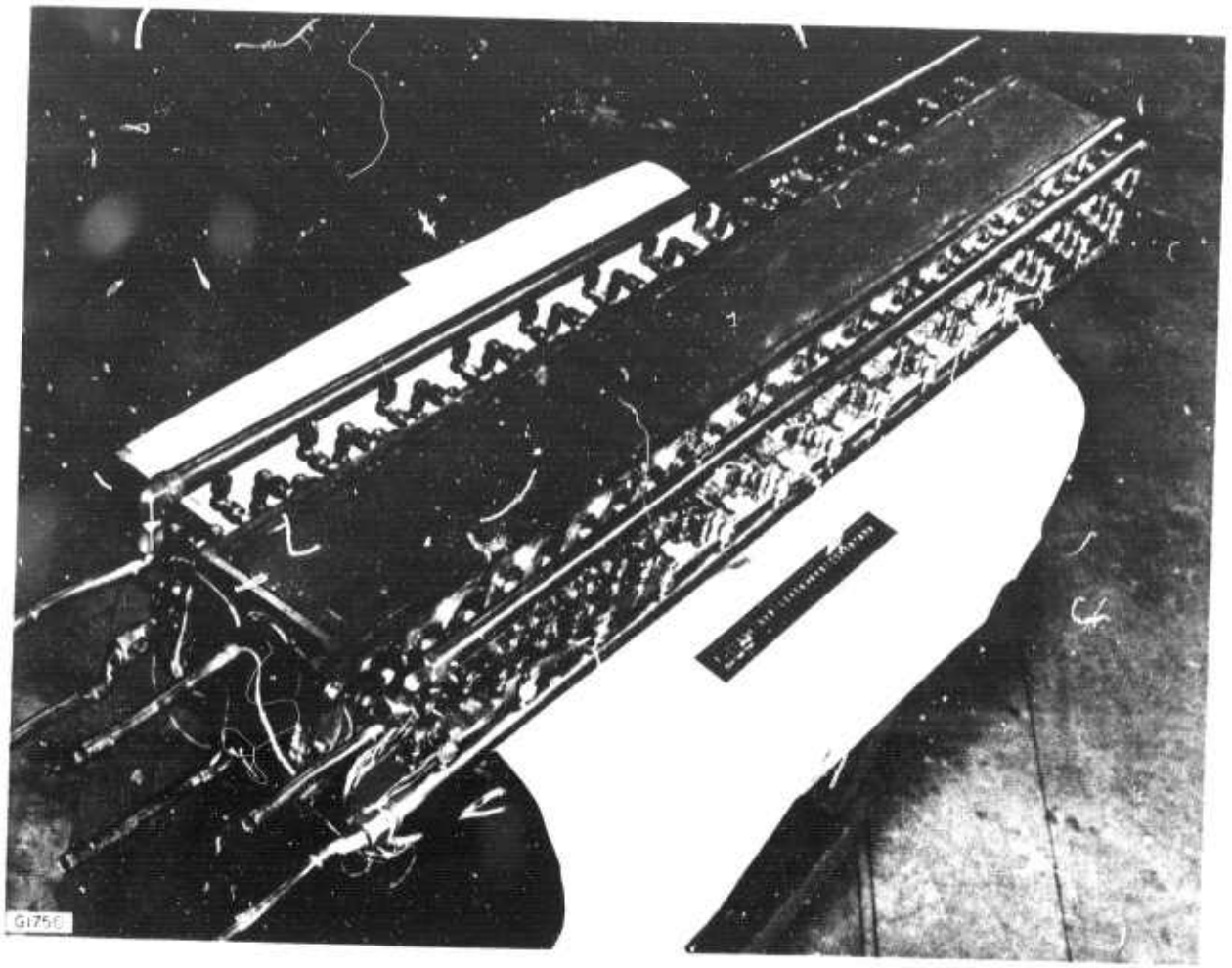

Fig. 9 Photograph of the Mk II CO Laser Heat Exchanger

## 4.0 MEDIUM QUALITY

Interferometric measurements of the cold flow medium homogeneity in the completed laser cavity have been performed. A conventional Mach-Zehnder interferometer was employed for these investigations and the optical configuration is described in a previous report.[20] Measurements were performed first without power input to determine whether the electrode installation had substantially interfered with the flow uniformity. Previous flow measurements without electrodes present demonstrated the need for certain modifications in order to improve the initially unsatisfactory medium uniformity to a level compatible with diffraction limited performance.[21] The introduction of a stainless steel screen above the heat exchanger eliminated turbulence originally present in the gas flow which was thought to be due to coalescing jets emerging from the porous heat exchanger plates. The flow measurements indicated that the 500 cfm Stokes pump introduced pulsations into the gas flow and this was therefore eliminated from the system and a dump tank facility introduced.

The original flow homogeneity calculations predicted that at flow velocities in the region of 100 cm/sec with laminar development on the side walls, boundary layers of a suitable thickness would be established which would provide the necessary medium uniformity over the active volume of the discharge. However in practice the boundary layers were found to be excessively thick and more consistent with a turbulent rather than laminar development. Increases in flow velocity were found to reduce the thickness of the boundary layers, however the mechanical restraints imposed by the heat exchanger restricted the available range of operating velocities. Eventually a flow velocity of approximately 400 cm/sec was found to satisfy the medium uniformity requirements and to be compatible with the mechanical limitations of the system. These measurements and modifications have been fully described in a previous report[21] and resulted in a much improved medium quality which was compatible with diffraction-limited operation.

Figure 10a shows a cold flow interferogram taken at a pressure of 1/6 atms and with the heat exchanger at 100°K, (equivalent to a density of 1/2 amagat) and with the electrodes cooled to approximately 200°K. As in the previous[21] measurements refractive effects in the warmer boundary layers apparently displace the flow-walls outwards and exaggerate the thickness of the boundary layers. Similar refractive effects close to the electrodes render their outlines indistinct. The electrode locations are plainly visible in the vacuum interferogram shown in Fig. 10b. In the right side of Fig. 10b the anode electrode can be seen to protrude further beyond the flow-wall than does the cathode on the left side. The E-beam foil is flush with the flow-wall behind the cathode. Potential distribution calculations[21] showed that this asymmetric configuration relieved stress concentration in the electric field and minimized non-uniformities in the deposition of electrical energy into the gas.



Preceding page blank

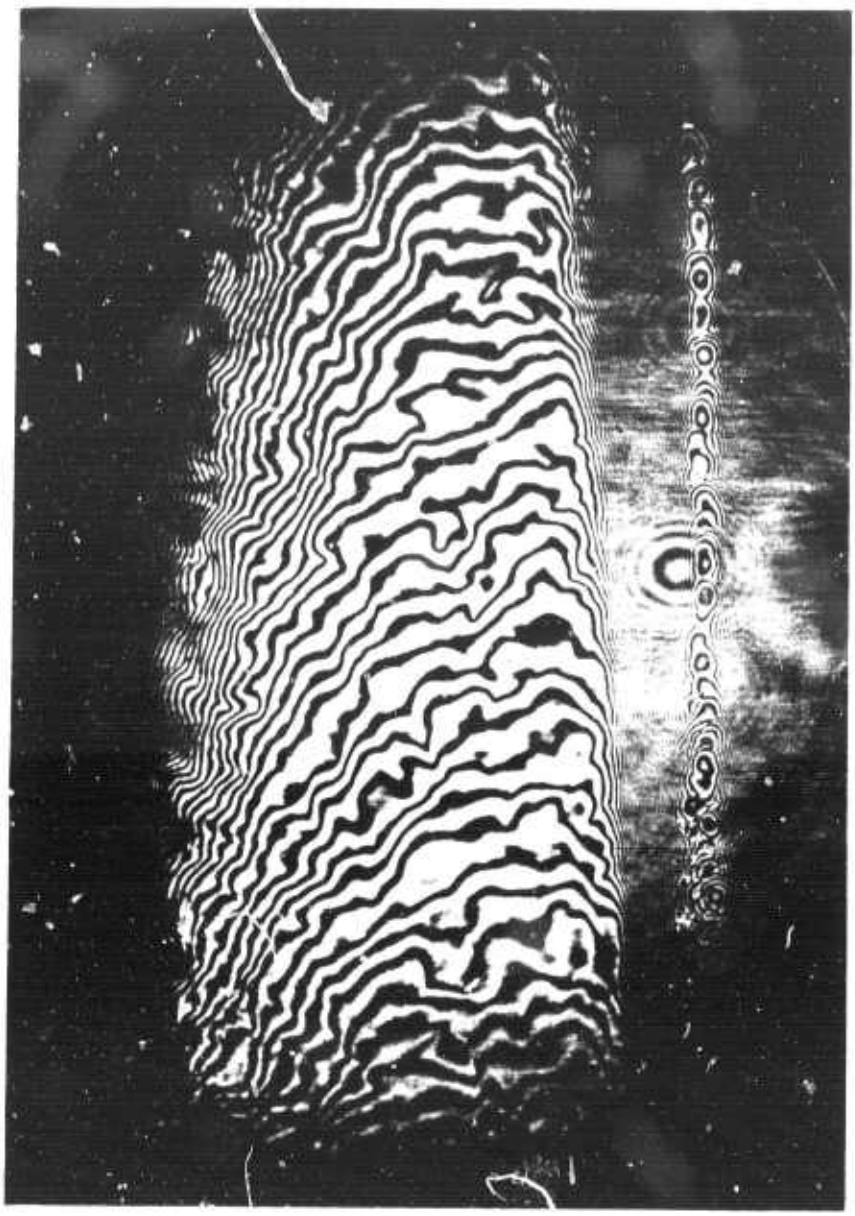

G1751

Fig. 10(a) Interferogram of the Medium Homogeneity in the Mk II Cavity Taken at a Pressure of 1/6 atms at a Temperature of 100°K and a Flow Velocity of 400 cm/sec. The electrodes were cooled to approximately 200°K.

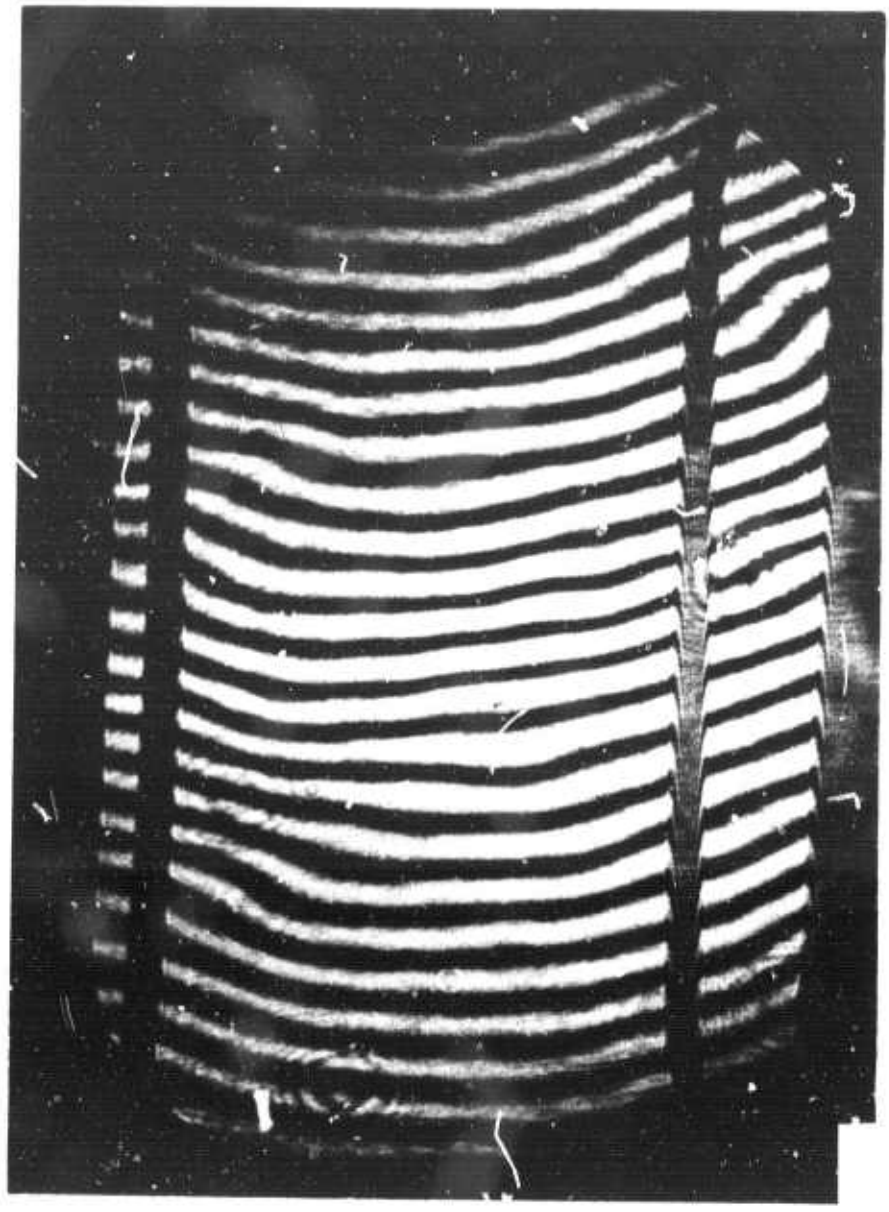

G1752

Fig. 10(b) Vacuum Reference Interferogram for Figs. 10(a) and 10(c)

The inclined fringes visible in Fig. 10a were observed in earlier flow tests and were ascribed to a small temperature gradient across the heat exchanger. At that time it was pointed out that such a gradient in the medium could be compensated by introducing a suitable tilt in the cavity optics. This is verified in Fig. 10c which was photographed under similar conditions to Fig. 10a but with one interferometer mirror tilted to compensate for the temperature gradient in the medium. The original design goal was to achieve 1.5 times diffraction limited quality in the cold gas medium which under these experimental conditions corresponds to a maximum variation in optical path equivalent to one fringe at 5000 Å. Figure 10c shows that this criterion has been met over approximately 90% of the volume contained within the electrodes.

These measurements were then repeated with power into the cavity. Interferograms were taken at a variety of elapsed times after termination of a 60 $\mu$sec discharge pulse. Figures 11a and 11b are cold flow interferograms taken at 1/6 atm pressure and at a gas temperature of approximately 80°K corresponding to a density of 1/2 amagat. The vacuum interferogram is shown in Fig. 11c. The excitation pulse length was 60 $\mu$secs during which approximately 5000 joules were deposited in the gas corresponding to a pumping rate of 5-6 kwatts/cm$^3$. Figure 11a was taken at the end of the discharge pulse and Fig. 11b 40 $\mu$secs later. Both interferograms show degradation of the medium due to acoustic wave distrubances propagating towards the center of the cavity. The reduction in width of the central good portion of the medium as the acoustic waves propagate across the cavity is clear from a comparison of Figs. 11a and 11b with the zero power input intergerogram shown in Fig. 10c. During the discharge pulse energy is uniformly deposited in the cavity producing bulk heating of the medium and thus a pressure increase occurs within the discharge region. Since the medium behind the electrodes is not similarly heated a pressure gradient is developed across the electrodes leading to a net outward motion of the gas through the open electrode structures. These acoustic wave disturbances are visible as rarefraction waves in Figs. 11a and 11b propagating inwards from the electrodes. An additional feature appearing as an abrupt change in gradient is visible on the leading edge of the cathode wave. This is attributed to the intense heating which occurs in the cathode fall region.

Interferograms similar to Figs. 11a and 11b have been analyzed to yield the density gradients across the cavity due to the acoustic waves. Figure 12 shows such a plot in terms of the fractional density change $\Delta\rho/\rho$. The density gradients associated with the acoustic disturbances will affect the spatial profile of the laser beam by causing refractive effects. These effects have been previously reported in studies of high power pulsed electric CO lasers[3] and have been shown to cause as much as a 25% power reduction in the intensity of the far-field central spot.

Near field burn patterns such as those shown in Figs. 13a and 13b show narrower regions of energy extraction in the vicinity of the electrodes, than would be expected from the extraction region geometrically defined by the resonator design. This is particularly noticeable in the region adjacent

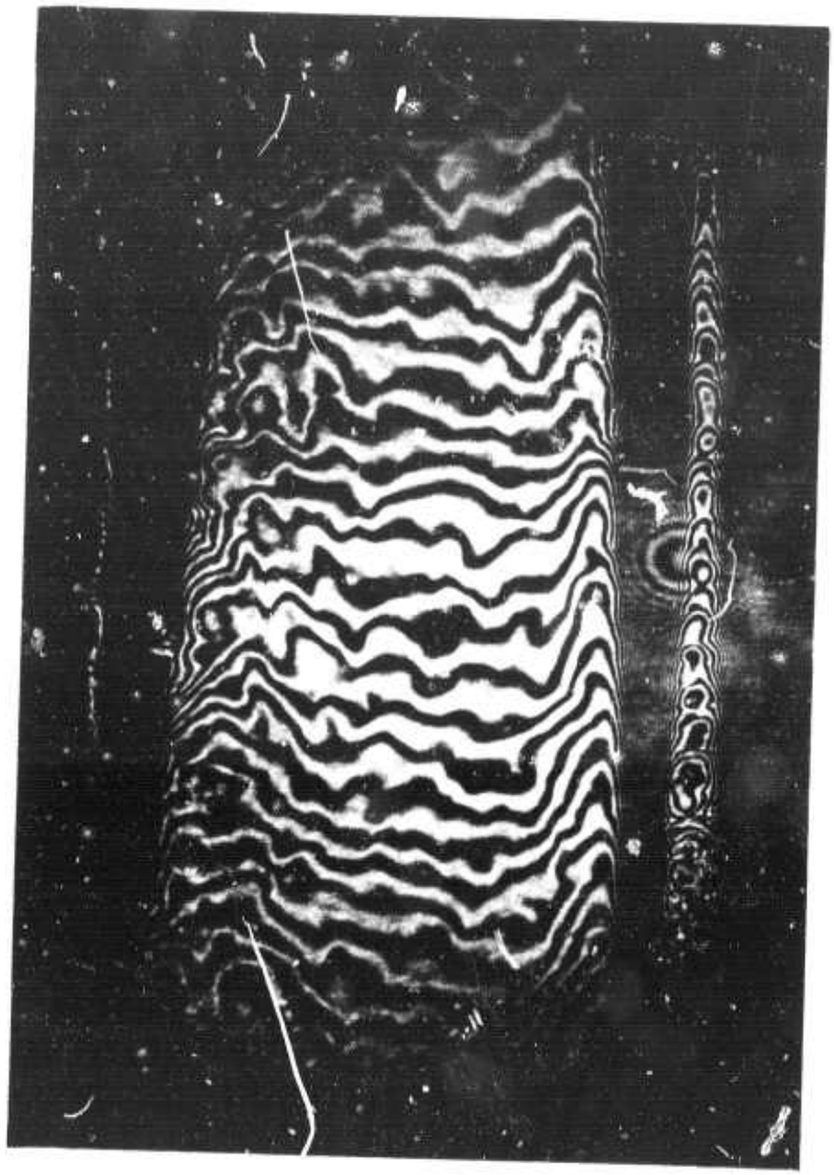

G1753

Fig. 10(c) Cold Flow Interferogram Taken under Identical Conditions to Fig. 10(a) but with an Interferometer Mirror Tilted to Compensate for the Transverse Temperature Gradient

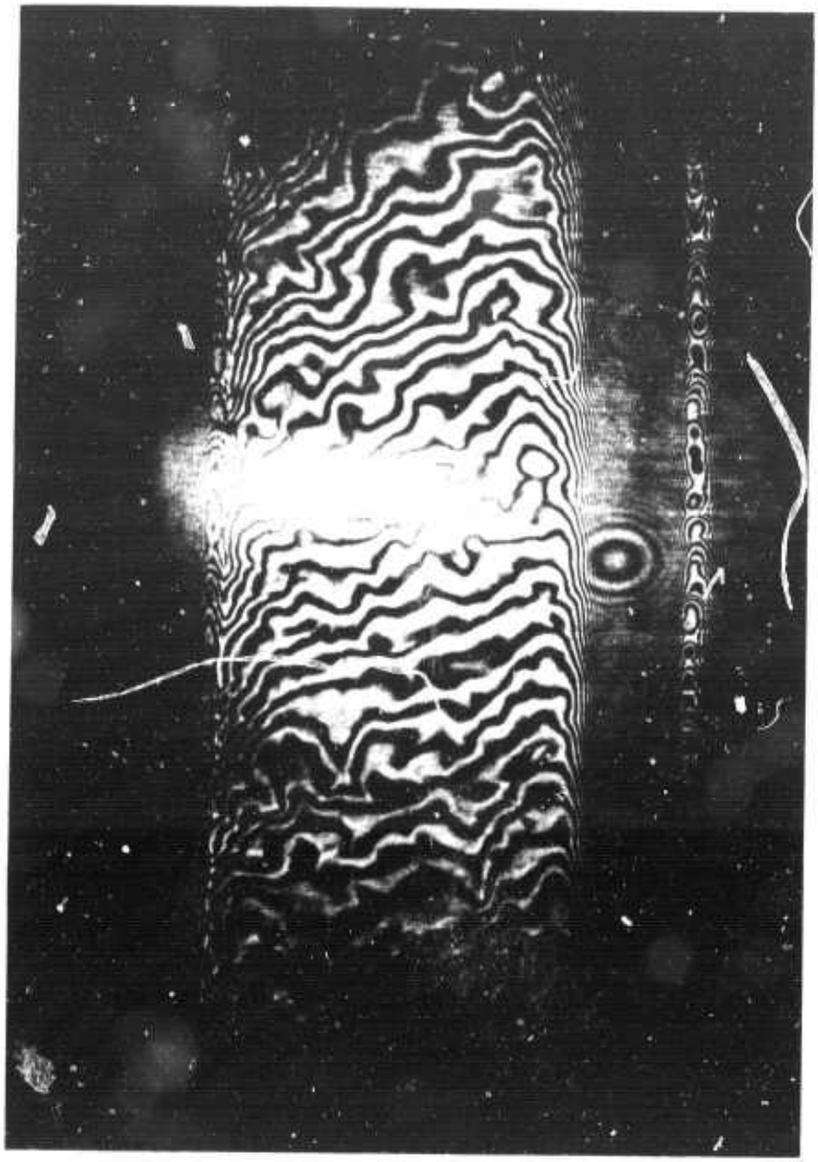

GI7541

Fig. 11(a) Cold Flow Interferogram Taken at the Termination of a 60 $\mu$sec Electric Discharge Pulse at 1/6 atms and at 80$^{o}$K

Reproduced from
best available copy.

G1754

Fig. 11(b) Cold Flow Interferogram Similar to Fig. 11(a) but Taken 40 $\mu$secs after the Termination of a 60 $\mu$sec Discharge Pulse

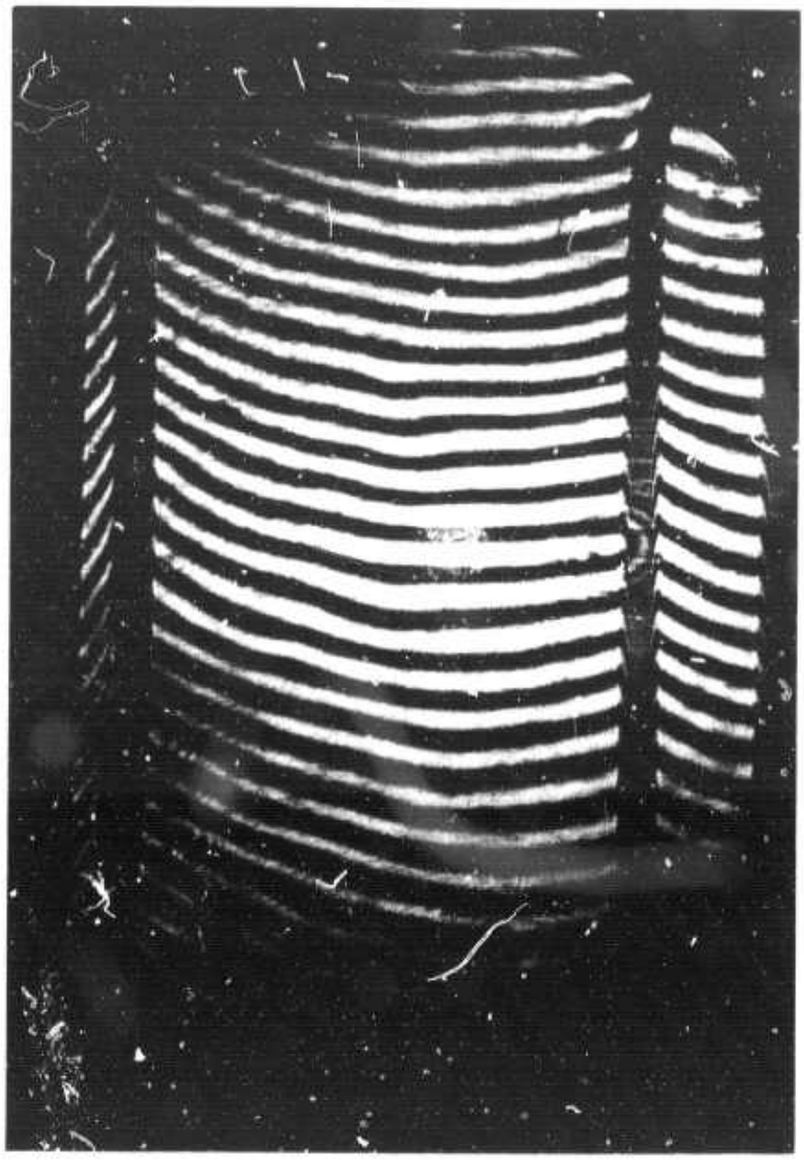

GI756

Fig. 11(c) Vacuum Reference Interferogram for Figs. 11(a) and 11(b)

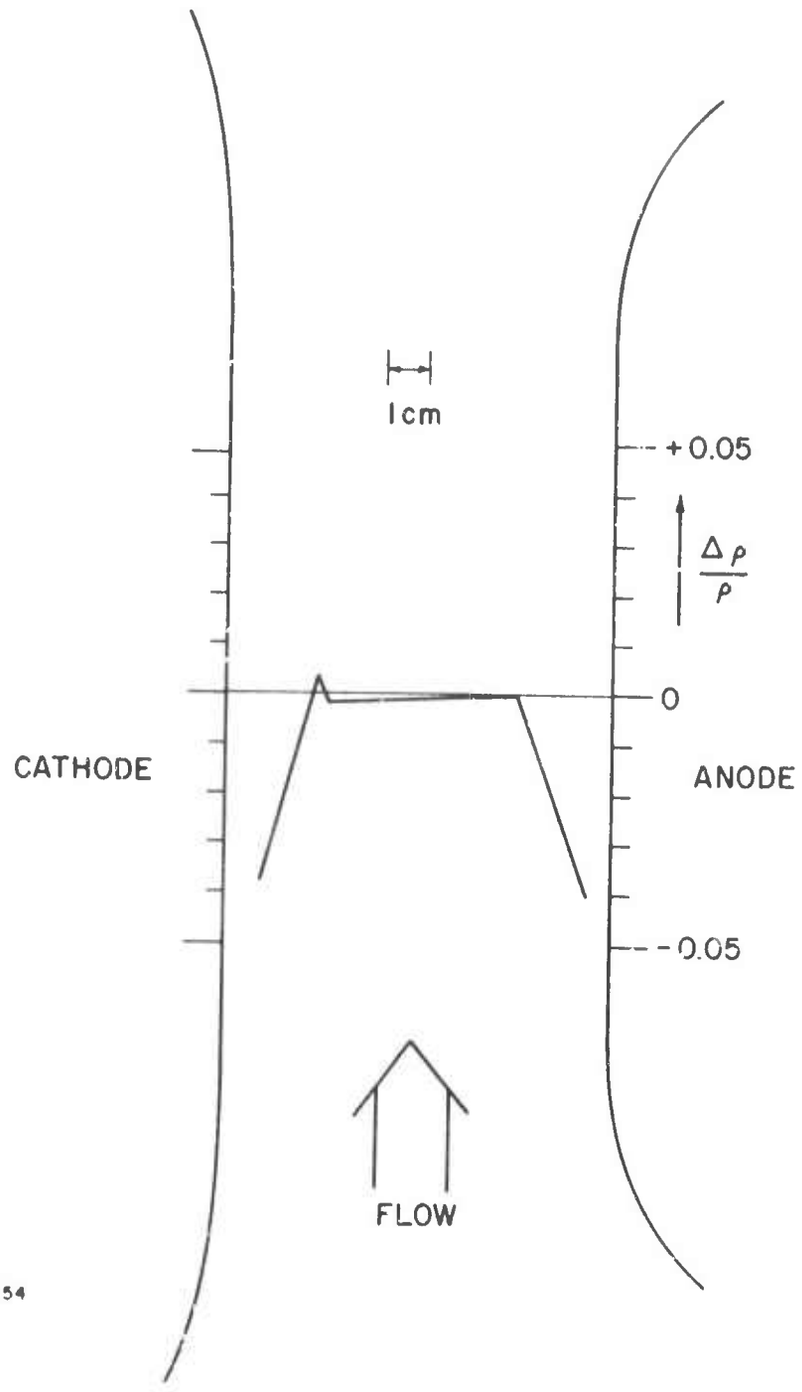


Fig. 12 Profile of the Fractional Density Change $\Delta\rho/\rho$ across the Laser Cavity Due to Acoustic Wave Disturbances at the Termination of a 60 $\mu$sec Discharge Pulse

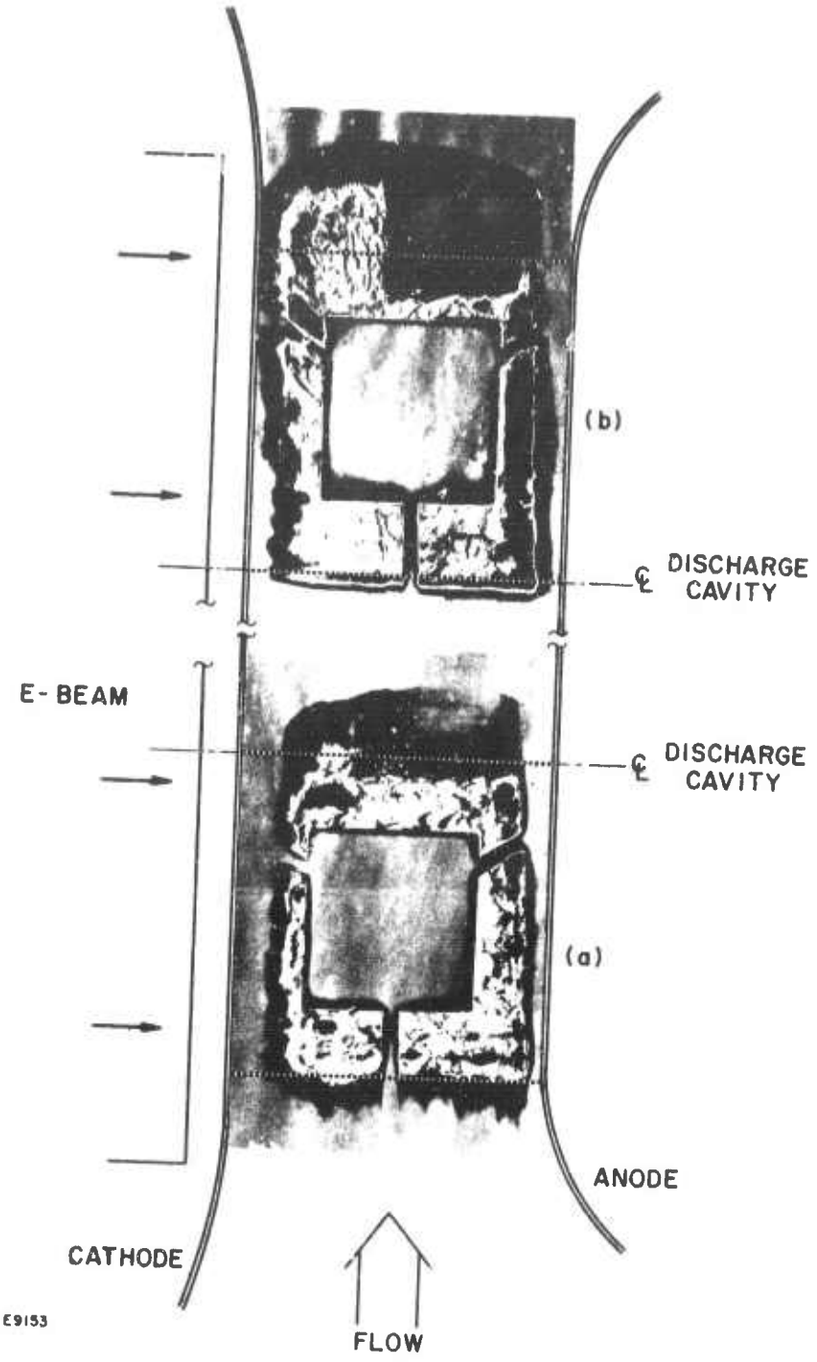


Fig. 13(a) and (b) Near Field Burn Patterns Obtained with Energy Extraction Separately from the Lower and Upper Halves of the Cavity, Respectively. The outline of the square output coupling mirror is visible in the center of each pattern.

to the cathode. This is a manifestation of the acoustic wave refraction. Under equivalent pumping conditions the magnitude of this effect is anticipated to be less than in those studies[22, 23] previously reported since the duration of the laser output pulse is considerably shorter in this device.

Acoustic wave measurements were also performed at 1/12 atms pressure. Typical interferograms are shown in Figs. 14a and 14b. The pumping conditions are as previously described. Figure 14a was obtained at the termination of the discharge pulse and Fig. 14b 110 $\mu$secs later. Clearly in Fig. 14b the acoustic waves have completely interacted with the medium completely degrading the quality. The vacuum reference pattern is shown in Fig. 14c. Interferograms taken under flow conditions similar to those used for Fig. 14a and Fig. 14b but without power into the medium indicated that the basic flow homogeneity was at least a factor of two better than that obtained at 1/6 atms pressure (1/2 amagat).

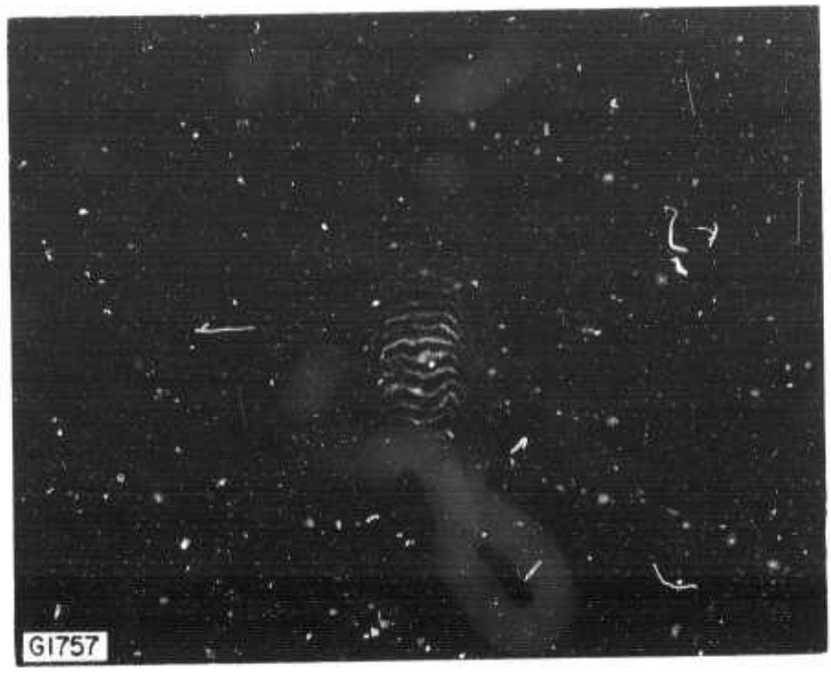


Fig. 14(a) Cold Flow Interferogram of the Medium Homogeneity at 1/12 atms and at 80°K. The interferogram was taken at the termination of a 60 $\mu$sec discharge pulse.

Reproduced from
best available copy.

GI738

Fig. 14(b) Cold Flow Interferogram Similar to Fig. 14(a) but Taken 140 $\mu$secs after the Termination of a 60 $\mu$sec Discharge Pulse

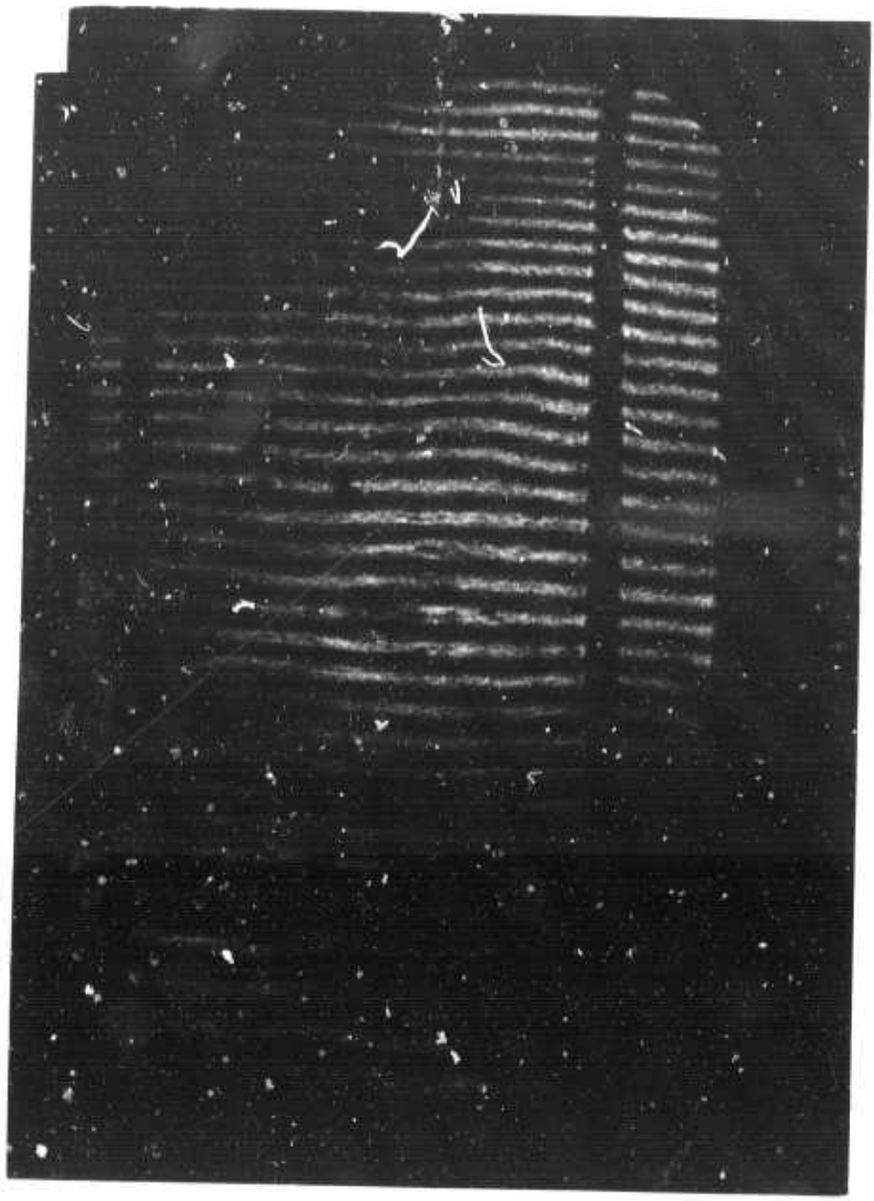


Fig. 14(c) Vacuum Reference Interferogram for Figs. 14(a) and 14(b)

# 5.0 EXPERIMENTAL RESULTS

This section describes experimental measurements of laser energy and efficiency, beam quality including near-field diffraction burn patterns, spectral distribution in the lasing pulse and small signal gain measurements obtained with the two discharge cavities developed under this program. Since most of the results obtained with the original 20 liter discharge system have been described in previous reports[24-27] those results are only briefly summarized in the present section. More detailed description is given of the results obtained with the new 16 liter discharge cavity which was designed to produce a near diffraction limited beam as described earlier in this report. A photograph of the pulsed electric CO laser with the 16 liter cavity is shown in Fig. 15.

## 5.1 PULSE ENERGY AND EFFICIENCY MEASUREMENTS

Measurements of total pulse energy and overall electrical efficiency were made with both flow systems (described in Section III) using stable and unstable resonator cavities. The stable resonator employed a 30% hole-coupled output mirror together with a 5 meter radius full reflector. Confocal unstable resonators were also used with most of the experimental data being obtained with a 72% coupled square output mirror. The thermionic electron gun used in these experiments was the same for both discharge cavities. The electron beam cross section was 20 cm x 100 cm with a maximum total electron beam current of approximately 20 amps after the foil corresponding to 10 milliamp per square cm. Both CO-Ar and CO-$N_2$ mixtures were employed in these experiments, the gas being precooled to liquid nitrogen temperature for most of the experiments. Some experimental measurements were also made in the 20 liter system using CO-$N_2$ and CO-Ar mixtures at room temperature. The typical gas pressures were approximately 120 torr with the pulse length variable from 20 to 100 microseconds.

Pulse energies in excess of 1000 joules were obtained with the 20 liter discharge cavity as shown in Table III. The maximum measured efficiency of approximately 20% was low in comparison with the predicted 50% electrical efficiency. This discrepancy is thought to be primarily related to the very poor thermal nonuniformity in the 20 liter system.[24] Although the gas was preconditioned to approximately 80 or 90°K interferometric measurements suggested that the minimum gas temperature in the 20 liter cavity was approximately 140°K with large gradients toward the walls. Near field burn patterns obtained with a 50% coupled unstable resonator further confirmed the nonuniform density and excitation in the system.[25]

Significantly higher electrical efficiency was measured with the recently developed 16 liter discharge cavity using both the stable and unstable resonators. Because of the large optical cross section in these devices,

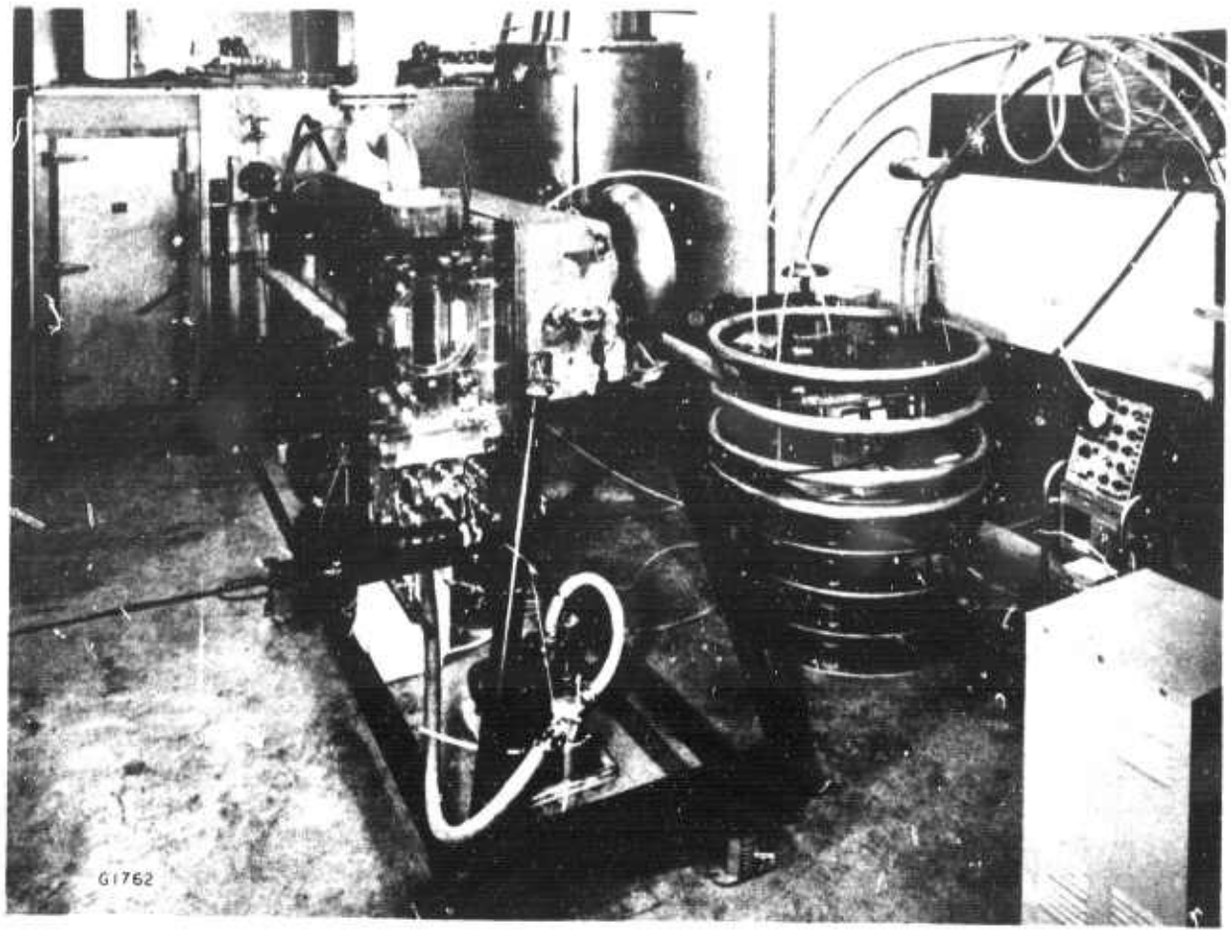


Fig. 15 Photograph of Mk II Pulsed, High Pressure CO Laser Facility

TABLE III

PERFORMANCE CHARACTERISTICS OF 20 LITER DISCHARGE CAVITY

Mixture ratio 20% CO: 80% Diluent

Density ~ 1/3 amagat

| Temperature* (°C) | Diluent | Sustainer Electric Field (kV/cm) | Laser Output (joules) | Discharge Pulse Length ($\mu$secs) | Efficiency** (%) |
|---|---|---|---|---|---|
| -140 | $N_2$ | 2.5 | 1500 | 90 | 20 |
| | Ar | 1.3 | 1700 | 90 | 19 |
| 20 | $N_2$ | 3.0 | 700 | 80 | 6 |
| | Ar | 2.0 | 200 | 40 | 4 |

*Estimated minimum temperature based on interferometry and thermocouple measurements.

**The Efficiency is defined as the ratio of the measured lasing output energy to the entire energy deposited into the discharge, as determined from the discharge current and voltage waveforms.

10 cm x 20 cm nominally for the 20 liter system and 8 cm x 20 cm nominally for the 16 liter system, the $CaF_2$ windows were not large enough to cover the entire cross section and so measurements were made with only half the optical volume using the center line of the discharge as a boundary. By displacing the optical system it was possible to obtain measurements from each half of the discharge volume and these measurements indicated symmetry about the center line. Care was taken in these experiments to completely mask the optically inactive side of the cavity to prevent any cross talk.

Major difficulty was experienced with the anti reflection coating on the $CaF_2$ windows used in these experiments. These coatings were easily destroyed in the lasing experiments. As a result most of the measurements were made with uncoated windows or at most only one coated window. The lack of anti reflection coatings had only a relatively small effect on the output measurements and this effect has been included in estimating the overall electrical efficiency in these experiments.

Figure 16 shows some typical oscillograms for lasing experiments in 20% CO- 80% $N_2$ with the 16 liter discharge cavity. The difference in the voltage and current wave forms between these oscillograms results from different configurations used in the capacitor tank which supplies the energy to the electron-beam-sustained discharge. In some experiments, (Fig. 16a) the capacitors were wired in parallel to provide minimum voltage drop and uniform power input during the pulse, while other experiments (Fig. 16b) were performed with the capacitors wired in series thus providing a relatively high initial voltage but with a very large droop in this voltage (and consequently in the power input). The highest electrical efficiencies were generally obtained with the latter configuration in which the power input is very high initially. This corresponds to operating at somewhat higher E/N as compared with the uniform power input experiments. Table IV summarizes the results obtained in the new discharge cavity.

The laser pulse energy was measured with an anodized aluminum calorimeter. The surface of this device was machined with 30° included angle grooves covering the entire surface in order to increase the absorption of the 5 micron radiation as described in an earlier report.[28] Because of the relatively high laser flux some surface ablation can take place from the calorimeter as evidenced by discoloration of the surface. Since this tends to underestimate the pulse energy several measurements were made in which a $CaF_2$ beam splitter was used in the main laser beam to reflect approximately 6% of the incident energy onto the calorimeter, thereby reducing the flux density onto the calorimeter. Both energy measurements agreed to better than 20%. A more serious problem in the energy measurements was indicated by burn patterns taken with heat sensitive paper mounted in the near field. Two extreme examples are shown in Figs. 13a and 13b. These burn patterns were produced with the 72% coupled unstable resonator using a square output mirror and should produce a square beam pattern. The black areas inside the light pattern represent complete burn through the heat sensitive paper. The burn pattern in Fig. 13a is fairly uniform with the exception of the dark area outside the main beam area in the upper left hand corner.

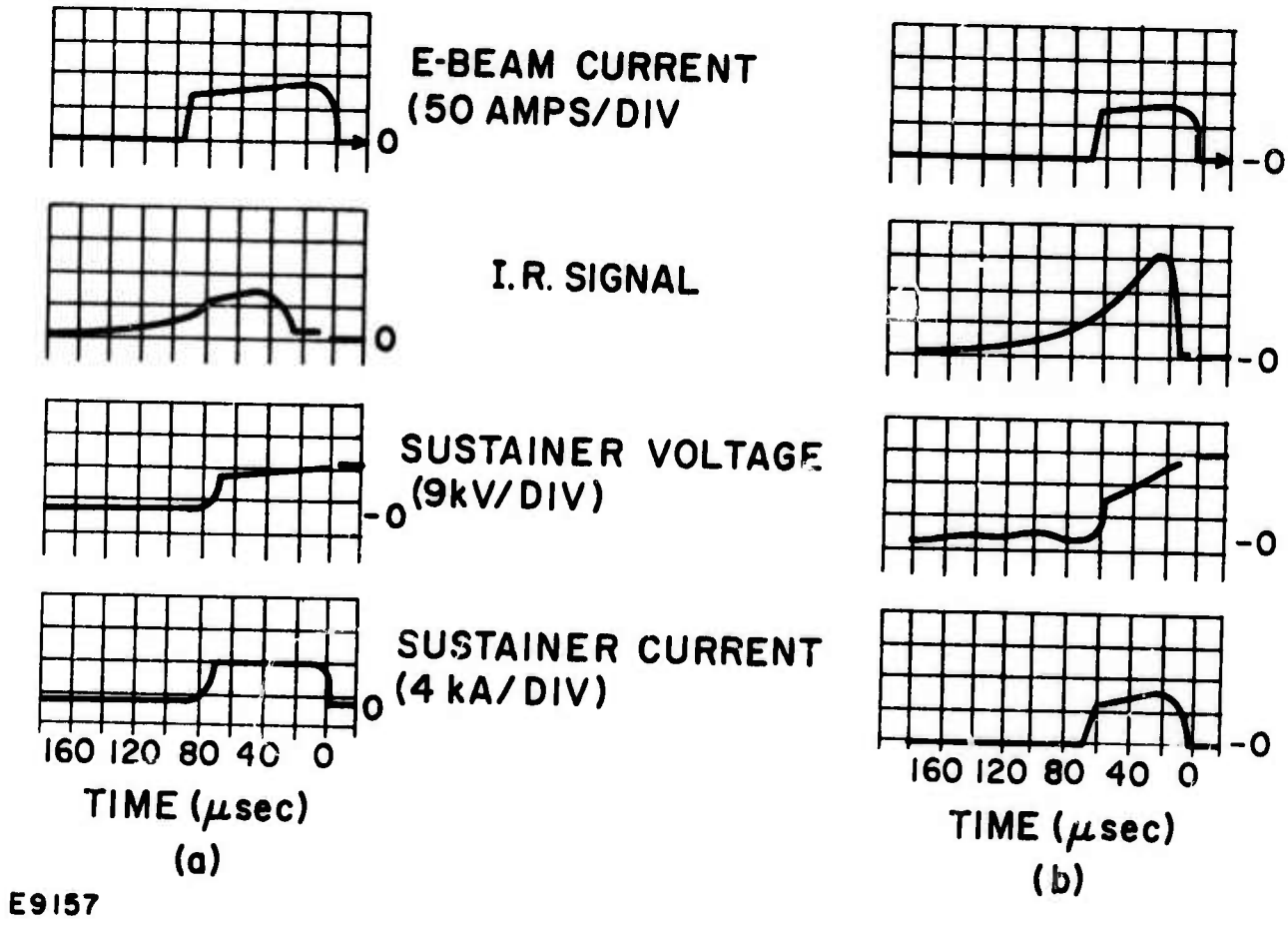


Fig. 16 Typical Oscillograms for Lasing Experiments in 20% CO - 80% Gas Mixtures with the Mk II Device.

In Fig. 16(a), the capacitor bank supplying discharge pumping power was wired in parallel; in Fig. 16(b), a series configuration was employed.

TABLE IV

PERFORMANCE CHARACTERISTICS OF 16 LITER TRANSVERSE FLOW CAVITY

Mixture ratio 20% CO: 80% Diluent

Density ~ 1/2 amagat

Temperature 80°K to 100°K

Beam quality better than 1.5 X diffraction limited

| Diluent | Sustainer Electric Field | Laser Output* | Discharge Pulse Length | Efficiency |
|---|---|---|---|---|
| | (kV/cm) | (joules) | ($\mu$secs) | (%) |
| $N_2$ | 2.5 | 1560 | 60 | 35 |
| Ar | 1.1 | 1010 | 40 | 38 |

*Output corrected for loss due to one uncoated window

This is accentuated in the extreme example in Fig. 13b in which the pattern is severely distroted in the upper half. This distortion results from parasitic oscillation which has robbed the gain medium in the upper part of the pattern. Careful masking of the optical region did not completely eliminate the parasitic oscillation which was further evidenced by burn areas on the mirror holders. Unfortunately, there was not sufficient time to investigate this parasitic oscillation properly and it is not clear whether this parasitic is due to reflection from the damaged or uncoated windows, or whether it is due to a reflection from the mirror holders themselves. Since it was not possible to completely eliminate the parasitic oscillation with external masking of the windows or mirror holders, this would suggest that the parasitic is initiated by some internal reflection in the cavity. These parasitic oscillations were evident in the experiments in both halves of the optical cavity and their presence tends to decrease the output lasing energy since the parasitic oscillation robs the active gain medium. The measured maximum electrical efficiencies may therefore be considered to underestimate the potential maximum efficiency in the system.

The temporal variation of the lasing pulse is in good agreement with the model prediction in both the delay time to reach threshold and the time to reach peak intensity. This is evident in Fig. 2 which compares the I. R. signal for the 20% CO-80% $N_2$ mixture of Fig. 16b with the prediction of the kinetic model. The peak fluxes have been normalized to unity for comparison of the waveforms. However the predicted efficiency is almost 60% compared with the measured 35%. A similar comparison for experiments in 20% CO-80% Ar mixtures is shown in Fig. 3. In this case the flux appears to decrease faster than predicted in the tail of the pulse and there were some experimental indications that the electrical efficiency was higher for somewhat shorter pulses, approximately 50 $\mu$sec.

Although the measurements of the temporal characteristics of the lasing pulse were found to compare very well with the model predictions a significant difference was observed between these results and those obtained by the Northrop program. The Northrop data for $CO/N_2$ mixtures[29] indicates that the duration of the lasing pulse greatly exceeds the electrical pumping pulse length and that the lasing pulse length increased as the ratio of CO to $N_2$ decreased. An explanation of these data in terms of V-V transfer from $N_2$ to CO was suggested and a calculation of the expected transfer rate expected to occur in the discharge supports this suggestion. However for $N_2$: CO ratios of 4: 1 the Northrop data indicates that approximately 50% of the lasing energy is extracted after the cessation of the lasing pulse. If V-V transfer from $N_2$ is thought to be responsible for this phenomena then the Northrop results imply that at the termination of the discharge approximately 50% of the energy is stored in the nitrogen vibrational manifold; however our model calculations predict that for this particular mixture the ratio of vibrational energy stored in $N_2$ compared to CO is only 20%. Experiments performed by Northrop with Ar/CO mixtures of similar dilutions certainly yielded shorter lasing pulse lengths in support of the V-V transfer mechanism, however even the duration of these lasing pulses still greatly exceeded the pumping pulse length and modeling the discharge pumping mechanism described by Northrop we are unable to duplicate their data

either experimentally or theoretically. Since the pumping rates employed in these experiments were generally higher than in the Northrop experiments, quenching of the vibrationally excited molecules by superelastic collisions with electrons was considered as a mechanism possibly responsible for this discrepancy since this process is not included in the model calculations. In order to test this hypothesis experiments were performed at reduced pumping rates by reducing the E-beam ionizer current. However over the pumping range investigated which overlapped with the Northrop mode of operation only a gradual reduction in both lasing energy and efficiency was observed, thus superelastic electron collisions are not thought to be responsible for the discrepancy.

The presence of impurities in the gas offers a further possible quenching mechanism by either V-V or V-T transfer. Common condensable vapors such as water if present in the gas originally would be expected to be efficiently trapped as the gas flows through the cryogenic heat exchanger. Leaks developed in the cavity would admit common atmospheric constituents and the presence of significant amounts of oxygen would soon become apparent due to the effect of electron attachment to oxygen which would cause a reduction in discharge current. Such effects were not observed and currently the discrepancy between the two sets of data remains unexplained.

## 5.2 BEAM QUALITY

An estimate of the beam quality can be obtained from the interferometric measurements discussed in Section IV as well as from diffraction phenomena exhibited in the near field burn patterns. In principle one would also like to measure the intensity distribution in the far field but time limitations in the program did not permit these experiments. Figure 17a and 17b show burn patterns illustrating Fresnel diffraction from the edges of the output mirror of the unstable cavity as well as from the anode plane. Figure 17a corresponds to a burn pattern taken 60 cm away from the output mirror and Fig. 17b is a burn pattern taken 500 cm away. The diffraction pattern from the output mirror is clearly evident in Fig. 17a in which the fringe spacing increases with distance away from the mirror edges, whereas in Fig. 17b the diffraction from the anode is evident and the fringe spacing decreases as one moves in from the right hand edge towards the output mirror.

The intensity contour for Fresnel diffraction at a straight edge can be readily predicted in terms of the distance between the source screen and diffraction edge and the wavelength. For a source effectively at infinity the distance along the screen is given by[30]

$$\ell = v\sqrt{\frac{b\lambda}{2}}$$

where b is the distance between the diffraction edge and the screen, $\lambda$ is the wavelength and v is the variable defining the Fresnel integrals. One can estimate the divergence angle of the beam which would cause complete overlap of the Fresnel diffraction at any fringe position. By counting the number of visible fringes, one can then make an estimate of this maximum divergence in order to estimate how many times diffraction limited the actual beam is.

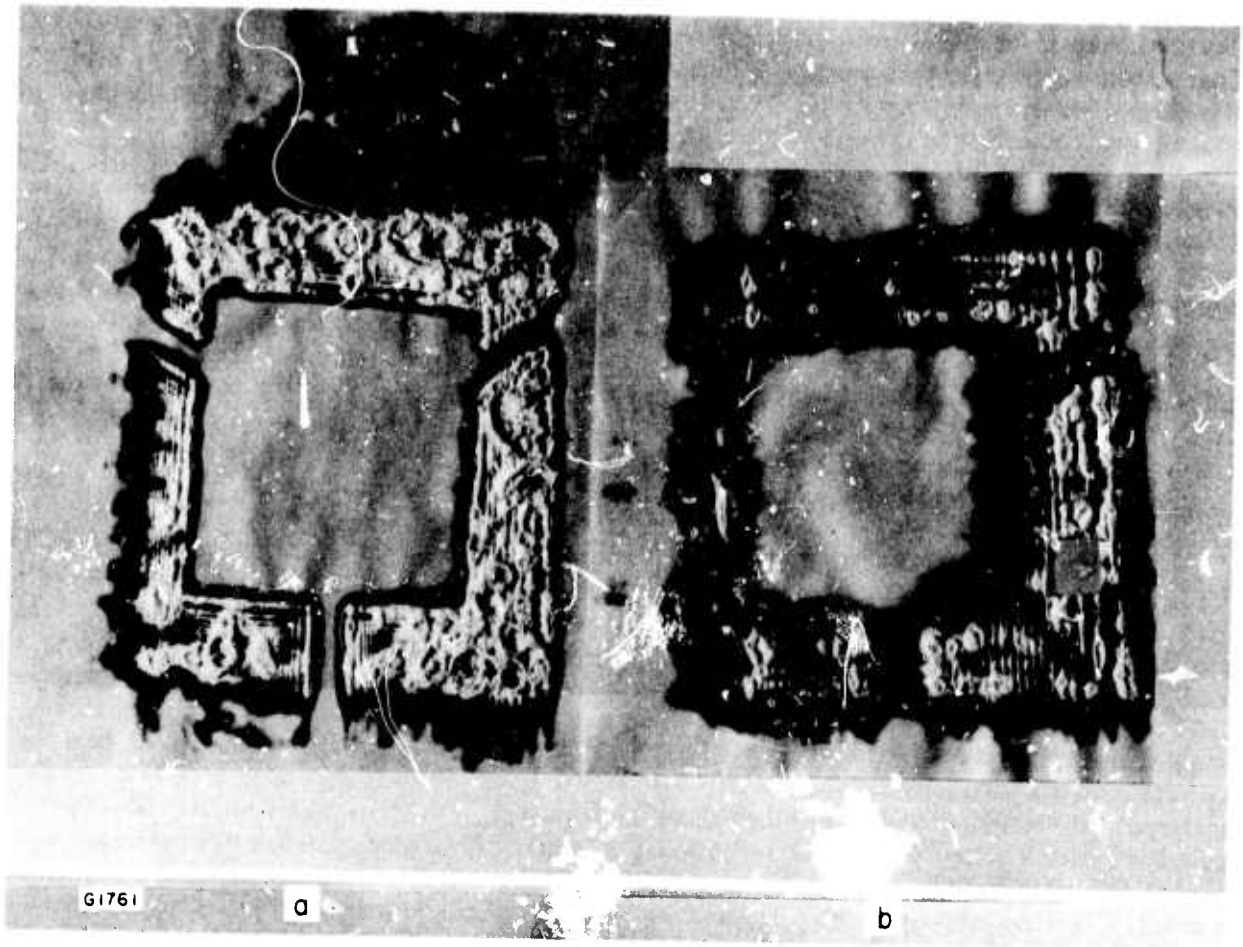


Fig. 17(a) and (b) Near Field Burn Patterns Illustrating Fresnel Diffraction from the Edges of the Output Coupling Mirror as well as from the Anode Plane. Figure 17(a) was taken 60 cm from the output coupling mirror and Fig. 17(b) 500 cm away.

Since the scale size on the screen increases as the square root of b, the distance between the diffraction edge and the screen (see the above equation), the fringe overlap criteria is clearly more sensitive with increasing distance from the screen. Thus from diffraction patterns such as shown in Fig. 17b one can readily show that the beam is at most 1.5 times diffraction limited. It should be emphasized that this is an upper bound. It is also important to notice from Figs. 17a and 17b that the diffraction pattern appears uniform over the entire burn area and runs from edge to edge indicating uniform beam quality over the entire optical cross section.

## 5.3 LASER SPECTRAL DISTRIBUTION

Some measurements were made of the output spectrum of the 16 liter discharge cavity using the unstable resonator with 72% output coupling. These measurements were made with both 20% CO diluted in $N_2$ and 20% CO diluted in Ar and at two different power input loadings for the CO-Ar mixtures. The measurements were performed by positioning the entrance slit of an Optical Engineering Spectrum Analyzer immediately behind a small aperture placed in the near field and photographing the spectrum displayed upon the fluorescent screen of the instrument.

Table V summarizes the tentative identification of the spectra and their relative strengths. In both gas mixtures, the model would predict that the lowest transition found to oscillate under the given power inpul loading should be the $4 \rightarrow 3$ transition, experimentally the $5 \rightarrow 4$ transition was the lowest observed. However, it should be pointed out that resonant self absorption, the effects of which are discussed in the following section may modify this output spectra significantly. One puzzling feature of the spectra in CO-Ar mixtures is the apparent lack of variation of the rotational level, J, with vibrational level as compared with the results in CO-$N_2$ in which the rotational level generally appears to decrease as the vibrational level increases in agreement with the predictions based on the kinetic model. We do not have any interpretation for this observation at present. It should also be pointed out that the spectral distribution is influenced by the amount of output coupling and that decreasing the output coupling would in principle lead to oscillation of lower rotational and possibly vibrational levels.

## 5.4 SMALL SIGNAL GAIN MEASUREMENTS

Small signal gain measurements were made in both discharge cavities by monitoring the intensity of a probe laser after transmission through the discharge. The probe laser was a stable/line-selected C.W. CO laser. Only a limited set of data was taken with the 16 liter thermally uniform discharge cavity but these measurements agree both in character and magnitude with the measurements taken in the 20 liter discharge cavity and described in detail in Refs. 25 and 27.

The variation of the peak small signal gain with the lower rotational level P(J) for various vibrational bands is shown in Fig. 18. Maximum gain

TABLE V

SPECTRAL MEASUREMENTS IN 20% CO - 80% $N_2$ OR Ar MIXTURES

P = 125 torr  T = 100°K

| DILUENT | $N_2$ | Ar | Ar |
|---|---|---|---|
| PEAK POWER LOADING WATTS/$CM^3$/torr CO | 250 | 250 | 250 |
| | 5P (14) VW | 5P (14) VW | 5P (12) M |
| | 5P (15) W | 5P (15) VW | 6P (11) M |
| | 6P (14) VW | 6P (14) W | 6P (12) M |
| | 6P (16) W | 6P (16) M | |
| | 7P (13) S | 7P (15) S | |
| | 7P (15) VW | 8P (14) M | |
| | 8P (12) VS | 8P (17) M | |
| | 8P (14) M | 9P (15) W | |
| | 9P (11) M | 9P (16) W | |
| | 9P (13) M | | |
| | 9P (16) W | | |
| | 10P (14) W | | |

RELATIVE INTENSITIES

VW - Very Weak

W - Weak

M - Medium

S - Strong

VS - Very Strong

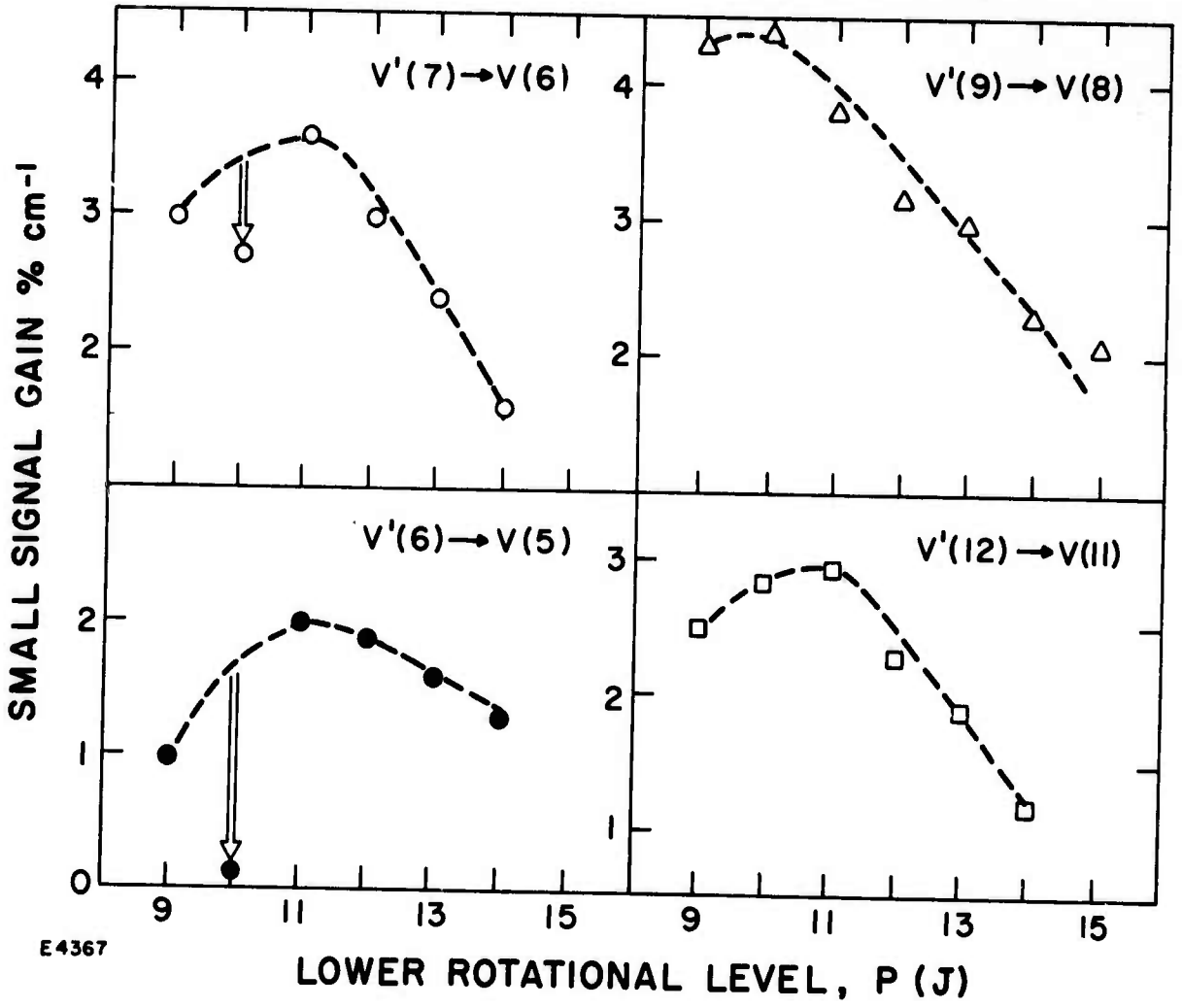


Fig. 18 Measurements of Maximum Small Signal Gain as Functions of Terminal Rotational Level for Various P-Branch Vibrational Transitions. The measurements were obtained on the Mk I CO laser.

of approximately 4 1/2% cm was measured on the 9P(10) and 8P(10) transitions in this set of data taken in the 20 liter discharge cavity. Most of the data for a particular vibrational transition showed a smoothly varying distribution as shown in Fig. 18. The 5P)12), 5P(13), 6P(10) and 7P(10) transitions did not conform to this pattern and exhibited anomalously low gain. The displacements of the 6P(10) and 7P(10) data points from the corresponding smooth curves are indicated in Fig. 18 by the vertical arrows.

Typical oscillograms of the temporal gain behavior together with the discharge current waveform are shown in Fig. 19. The 9P(9) oscillogram is representative of all except those transitions with anomalously low gain. Lacina and McAllister[31] have attributed the absence of several lasing transitions to resonance absorption of those transitions by overlapping transitions. The extent of the overlap and the population distribution determine the degree of absorption. For example, the 6P(10) transition is overlapped by the 8P(3) transition, the separation of the unshifted lines being .11 $cm^{-1}$ and for the present experimental conditions the lines are pressure broadened with the half width of approximately .03 $cm^{-1}$ (FWHM). Thus absorption occurs due to overlap between the wing of the 8R(3) transition and the line center of the 6P(10) line. Since the peak of the rotational distribution is expected to occur close to the J = 7, the absorption will mainly occur by overlap with transitions involving lower rotational levels.

Figure 20 shows the predicted dependence of small signal gain in each vibrational band as a function of P(J) for our estimated experimental conditions. In contrast to the measurements, the maximum gain is predicted to occur on the 12P(10) transition and magnitudes of the peak gain on all transitions are calculated to be significantly higher than the measured values. Resonance absorption of the 6P(10) and 7P(10) transitions by the 8R(3) and 9R(3) levels respectively was included in the gain calculation. The effect is indicated in Fig. 20 by the vertical arrows which indicate the extent of the gain suppression. The predictions are in qualitative agreement with the measurements shown in Fig. 18.

Similar results were obtained with the 16 liter discharge cavity. One puzzling feature of all the gain experiments is the observation that the majority of the transitions do not exhibit the initial absorption predicted by the kinetic model calculations and shown in Fig. 4. (The anomalous transitions exhibit initial absorption followed by either anomalously low gain or further absorption at later times in contrast to the majority of the transitions which exhibit gain initially which then decays to zero or occasionally to absorption). It should be emphasized that in all these experiments the signal to noise detection sensitivity was sufficient to reveal absorption levels as low as .2% per cm which is well below the predicted values. This disagreement between measurement and calculation with regard to initial absorption is not understood at present. Although the degree of absorption predicted by the kinetic model is sensitively dependent upon the detailed structure of the vibrational relaxation rates there is not justification at present for any significant variation in the assumed rate constants.

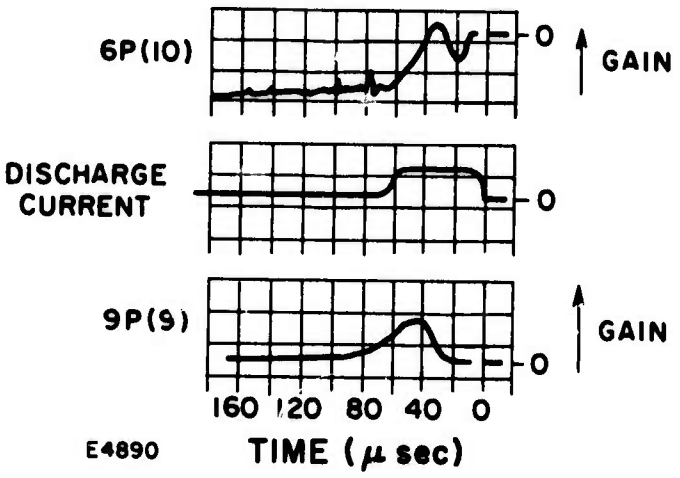


Fig. 19 Temporal Variation of the Probe Laser Intensity while Oscillating on the 6P (10) and 9P (9) Transitions. The discharge current pulse is shown at the center of the figure. These measurements were performed on the Mk I CO laser.

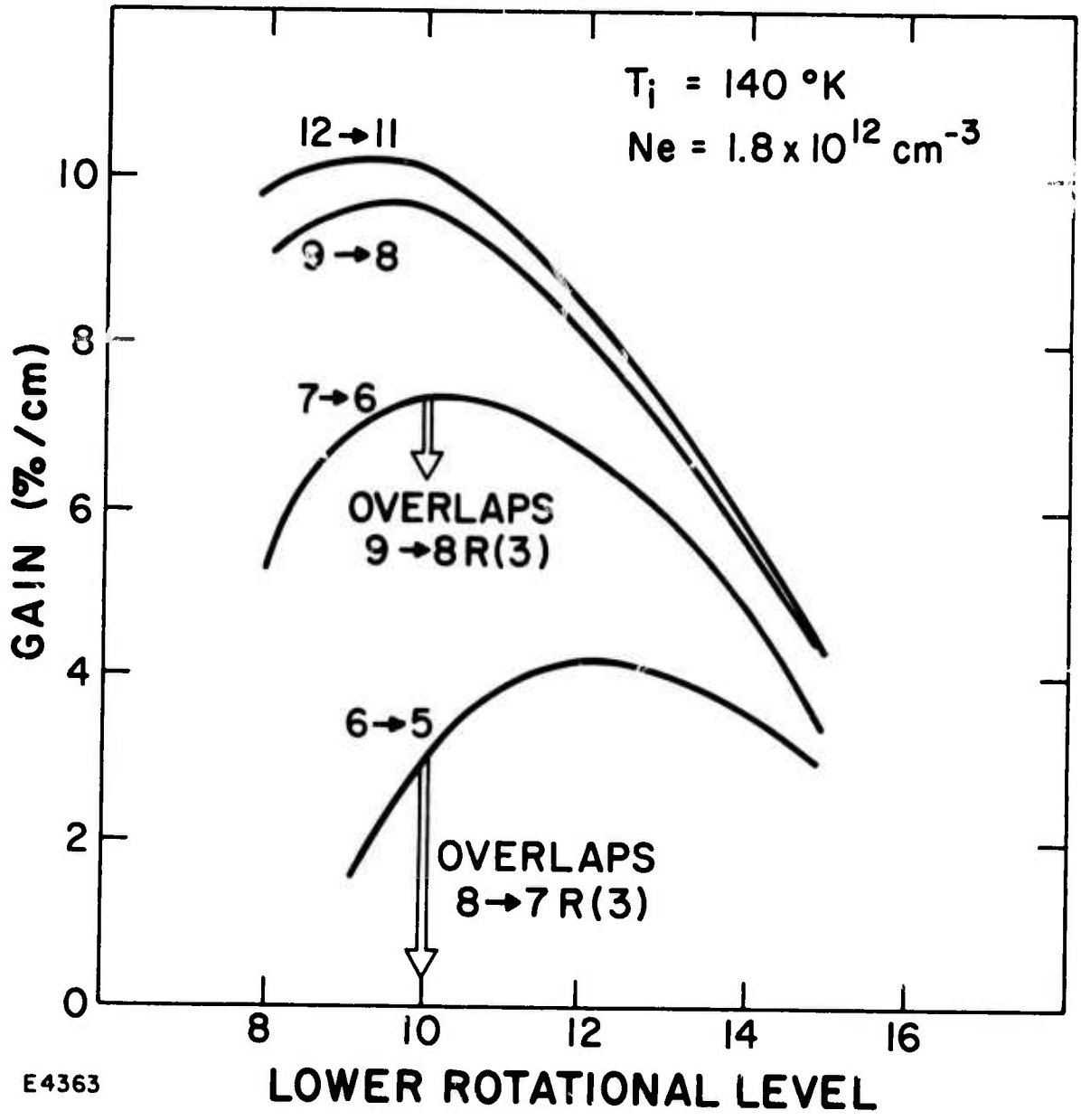


Fig. 20 Predictions of Maximum Small Signal Gain for Various P-Branch Transitions. The arrows indicate the extent of gain suppression on the 6P (10) and 7P (10) transitions when resonance absorption is included in the calculations.

The characteristic trends of the temporal gain behavior predicted by the kinetic model such as times to reach threshold and peak gain as a function of the vibrational and rotational levels were qualitatively confirmed. An example of this is shown in Fig. 21 in which the time to reach maximum gain for the 7-6 transition is shown as a function of the lower rotational level. The experiments also indicated that higher lying vibration levels require longer time to reach threshold and peak gain lending additional support to the energy transfer mechanism proposed for establishing partial inversions.

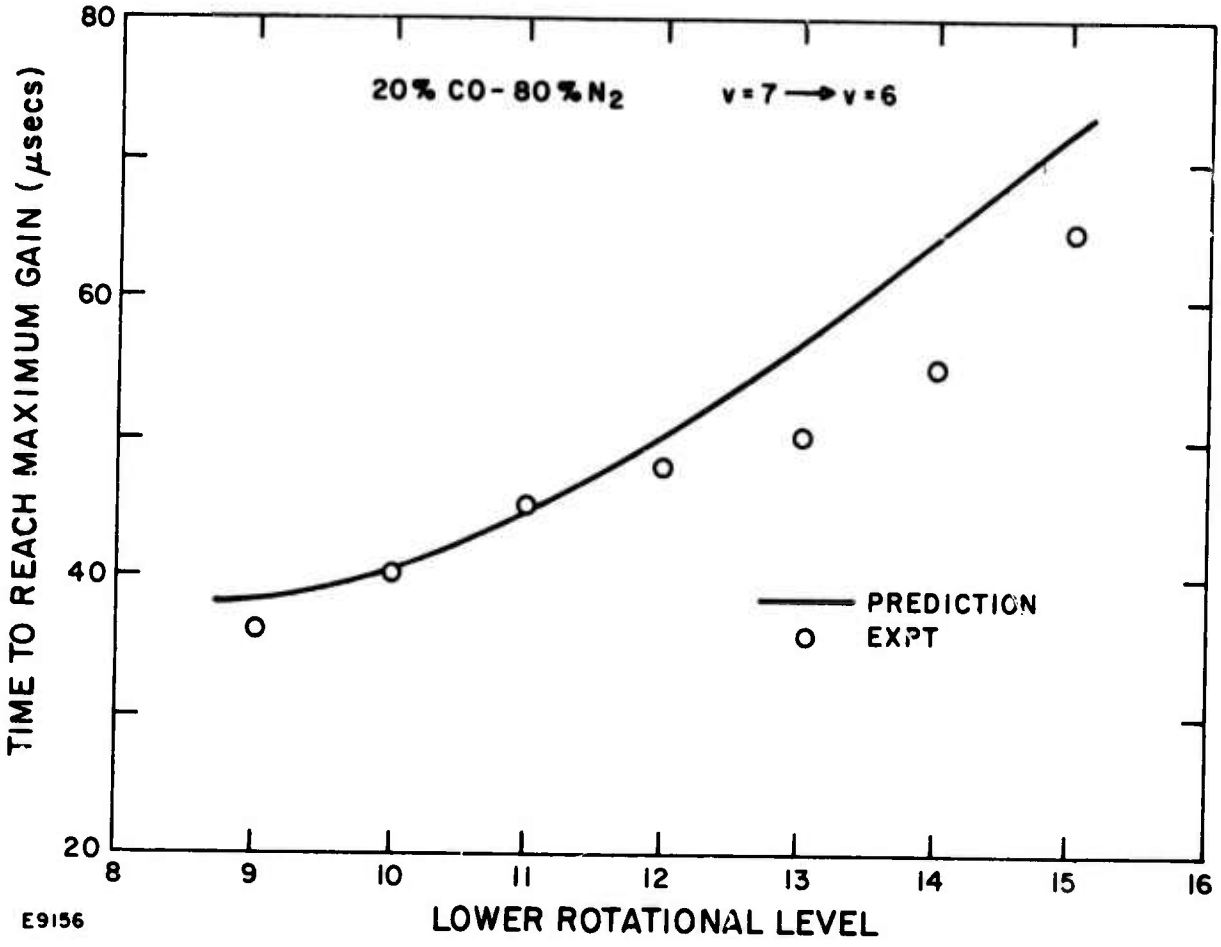


Fig. 21 Comparison of Predicted and Measured Time to Reach Maximum Gain as a Function of 7P (J). The measurements were made on the Mk I CO laser.

# 6.0 RECOMMENDATIONS FOR FUTURE WORK

During the course of this program a number of discrepancies were observed between the experimental results and the model predictions. In certain instances although experiment and theory were found to yield consistent results differences existed between these data and those from other laboratories.

Furthermore various experimental observation revealed unexpected behavior and suggested certain avenues of investigation to be pursued beyond the time available. In order to reconcile the discrepancies, to implement the modifications and improvements and to further pursue interesting results derived from the program the following suggestions for future work in the pulsed CO laser program are recommended.

## 6.1 MODEL CALCULATIONS

(a) Include effects of resonance absorption by overlapping transitions

(b) Treat the electron kinetics more completely by including superelastic electron collisions with excited species and treat the problem of electron excitation from vibrationally excited species to more highly excited vibrational levels exactly without recourse to the usual assumptions or approximations. An exact treatment of the excitation from excited states requires a knowledge of the relevant cross section. Theoretical calculations of these cross sections are presently in process; however an experiment has been devised which would supply the required data.

(c) A limited number of calculations were performed to investigate the spectral composition as a function of various parameters including gas temperature and power loading. A more complete analysis of this problem is desirable since the preliminary calculations indicate that by optimizing various parameters the atmospheric propagation characteristics of the laser beam could be significantly improved. This problem requires a knowledge of the atmospheric attenuation of CO laser radiation for which there are no experimental results; separate efforts should be encouraged to remedy this situation.

(d) Since currently preliminary new measurements of the cross sections for vibrational excitation in $N_2$ by electron impact reveal significant differences in magnitude compared with the previous data, efforts should be made to incorporate the new values into the kinetics calculations as soon as they become available in order to investigate to what extent these new values modify the previous parametric performance predictions.



Preceding page blank

## 6.2 PARASITIC CAVITY OSCILLATION

The burn patterns illustrated in Fig. 13 exhibit severe parasitic oscillations. More work is needed to identify and eliminate the surfaces responsible for these effects. Since window reflections are prime candidates for such parasitics particularly in high gain systems the following cavity modification is suggested. Instead of employing windows placed at normal incidence a parallel configuration tilted with respect to the lasing axis to form a rhombus shaped cavity would be desirable. It would be necessary to simultaneously reconstruct the heat exchanger in order to conform to the modified cavity configuration. Thus the porous plates would be rhombus shaped with the copper cooling pipes embedded parallel to the cavity windows, i.e. to the short dimension of the rhombus. Rather than employ Brewster angle windows which require prohibitively large samples of calcium fluoride a smaller angle of incidence would be employed. The 5 $\mu$ A.R. coatings recently developed by Northrop[32] would be employed to reduce the cavity losses.

## 6.3 SPECTRAL COMPOSITION VS GAS MIXTURE

Unexplained differences in spectral composition were observed using similar ratios of different diluents. These effects were not predicted by the model calculations and additional parametric performance measurements of this behaviour should be performed both with the two diluents previously employed (i.e. $N_2$ and Ar) and also with a variety of additional diluents.

## REFERENCES


1. Caledonia, G.E. and Center, R.E., J. Chem. Phys. 55, 552 (1971).

2. Center, R.E. and Caledonia, G.E., Appl. Phys. Letters 19, 211 (1971).

3. Cottrell, T.L. and McCowbrey, J.C., Molecular Energy Transfer in Gases, Butterworths, London (1961).

4. Rigrod, W.W., J. Appl. Phys. 36, 2487 (1965).

5. Hake, R.D., Jr. and Phelps, A.V., Phys. Rev. 158, 70 (1967).

6. Nighan, W.L., Appl. Phys. Letters 20, 96 (1972).

7. Schulz, G.J., Rev. Mod. Phys. 45, 423 (1973).

8. Ehrhardt, H., Langhans, L., Linder, F. and Taylor, H.S., Phys. Rev. 173, 222 (1968).

9. Boness, M.J.W. and Schulz, G.J., Phys. Rev. A8, 2883 (1973).

10. Jones, T.G., Byron, S.R., Hoffman, A.L., O'Brien, B.B. and Lacina, W.B., AIAA Paper No. 74-562, 7th Fluid and Plasma Dynamics Conference, Palo Alto, California, June 1974.

11. Rockwood, S.D., Brau, J.E., Proctor, W.A. and Canavan, G.H., IEEE J. Quantum Electron. QE-9, 120 (1973).

12. Center, R.E., J. Appl. Phys. 44, 3538 (1975).

13. Horton, R.L., Franklin, J.L. and Mazzeo, B., J. Chem. Phys. 62, 1739 (1975).

14. Center, R.E., IEEE J. Quantum Electron. QE-10, 208 (1974).

15. Boness, M.J.W. and Center, R.E., Appl. Phys. Letters 26, 511 (1975).

16. Powell, H.T., J. Chem. Phys. 59, 4937 (1973).

17. "Carbon Monoxide Laser, Semi-Annual Technical Report," Avco Everett Research Laboratory, Contract No. N00014-72-C-0030, November 1973.

18. Center. R.E., IEEE J. Quantum Electron. QE-10, 208 (1974).

19. "Carbon Monoxide Laser, Annual Technical Report," Avco Everett Research Laboratory, Contract No. N00014-72-C-0030, May 1974.

20. "Carbon Monoxide Laser, Semi-Annual Report," Avco Everett Research Laboratory, Contract No. N00014-72-C-0030, November 1973.

21. "Carbon Monoxide Laser, Semi-Annual Report, Avco Everett Research Laboratory, Contract No. N00014-72-C-0030, June 1975.

22. "High Power CO Laser, Quarterly Technical Report, Northrop Research and Technology Center, Contract No. N00014-72-C-0043, July 1974.

23. McAllister, G. L., Dragoo, V. G., Eguchi, R G., Applied Optics 14, 1290 (1975).

24. "Carbon Monoxide Laser, Annual Technical Report," Avco Everett Research Laboratory, Contract No. N00014-72-C-0030, May 1974.

25. "Carbon Monoxide Laser, Annual Technical Report," Avco Everett Research Laboratory, Contract No. N00014-72-C-0039, January 1975.

26. Center, R.E., IEEE J. Quantum Electron. QE-10, 208 (1974).

27. Boness, M.J.W. and Center, R.E., J. Appl. Phys. Letters 26, 511 (1975).

28. "Carbon Monoxide Laser, Final Technical Report Phase 1," Avco Everett Research Laboratory, Contract No. N00014-72-C-0039, April 1973.

29. "High Power CO Laser, Final Report," Northrop Research and Technology Center, Contract No. N00014-72-C-0043, March 1975.

30. Jenkins. F.A. and White, H.E., Fundamentals of Optics, McGraw-Hill, New York, Chapter 18 (1950).

31. Lacina, W.B. and McAllister, G., Appl. Phys. Letters 26, 86 (1975).

32. Rice, D.K., Private Communication.

## PUBLICATIONS, REPORTS AND PRESENTATIONS

### Publications


1. G.E. Caledonia and R.E. Center, J. Chem. Phys. 55, 552 (1971).
2. R.E. Center and G.E. Caledonia, Appl. Phys. Lett. 19, 211 (1971).
3. R.E. Center and G.E. Caledonia, Appl. Optics 10, 1795 (1971).
4. R.E. Center, J. Appl. Phys. 44, 3538 (1973).
5. R.E. Center, IEEE J. Quantum Electron. QE-10, 208 (1974).
6. M.J.W. Boness and R.E. Center, Appl. Phys. Lett. 26, 511 (1975).
7. R.E. Center and G.E. Caledonia, J. Appl. Phys. 46, 2215 (1975).


### Reports


1. "Carbon Monoxide Laser," Final Technical Report, Phase I, Avco Everett Research Laboratory, April 1973.
2. "Carbon Monoxide Laser," Semi-Annual Report, Avco Everett Research Laboratory, November 1973.
3. "Carbon Monoxide Laser," Annual Technical Report, Avco Everett Research Laboratory, May 1974.
4. "Carbon Monoxide Laser," Annual Technical Report, Avco Everett Research Laboratory, January 1975.
5. "Carbon Monoxide Laser," Semi-Annual Technical Report, Avco Everett Research Laboratory, September 1975.


### Presentations


1. R.E. Center, "High Pressure Pulsed Carbon Monoxide Laser," Conference on Laser Engineering & Applications, Washington, D.C., May 30 - June 1, 1973.
2. M.J.W. Boness and R.E. Center, "Observations of Small Signal Gain in a High Pressure Pulsed CO Electric Discharge Laser," 27th Gaseous Electronics Conference, Houston, Texas, October 22 - 25, 1974.

# APPENDIX A

## KINETICS

The basic physics describing the kinetic processes appropriate to the electrically excited CO laser are contained in the master vibrational rate equation for the density of molecules in each vibrational level. For pure CO or a mixture of CO and an inert diluent there is just one set of master equations appropriate to each vibrational level of the CO molecule. In the case of mixtures containing another diatomic molecule, such as CO-$N_2$ mixtures, it is necessary to use a similar set of master equations for each vibrational level of the $N_2$. For the electrically excited CO laser the master equation can be simply written in the form (for the CO molecules)

$$\frac{dN_v}{dt} = F_{v-1,v} - F_{v,v+1} - D_v + D_{v+1} + E_v + S_{v+1,v} - S_{v,v-1} \qquad (A-1)$$

where

$F_{v,v+1}$ is the net particle flux between levels v and v+1 resulting from V-V collisions

$D_{v+1}$ is the rate of deactivation from level v+1 as a result of V-T collisions and radiative decay

$E_v$ is the net rate of change of $N_v$ as a result of direct electron impact

$S_{v+1,v}$ is the rate of increase in $N_v$ resulting from stimulated emission.

These four terms are described in detail below, together with the assumptions involved in deriving their analytic form.

The V-V and V-T relaxation processes have been considered in detail in previous analysis of vibrational distributions in anharmonic oscillators (e.g., Ref. 3). The assumption is made that only single quantum transitions occur in collisional exchange and one can then write

$$F_{v,v+1} = \sum_M \sum_i \left[ k^{v,v+1}_{i,i-1} N_v M_i - k^{v+1,v}_{i-1,i} N_{v+1} M_{i-1} \right] \qquad (A-2)$$

$$D_{v+1} = \sum_M \left[ k^{v+1,v}_{V-T} N_{v+1} - k^{v,v+1}_{V-T} N_v \right] M + N_{v+1}/\tau_{v+1} \qquad (A-3)$$

where $k^{v,v+1}_{i,i-1}$ and $k^{v,v+1}_{V-T}$ refer to the rate constants for V-V and V-T exchange respectively, $\tau_{v+1}$ is the radiative lifetime of level v + 1 and M is the collision partner. The sources of the relevant rate constants have been described previously. (1) Theoretical calculations as well as recent



Preceding page blank

experiments[2-5] have shown that the intramolecular V-V processes are extremely rapid in CO. For atmospheric pressure discharges the characteristic V-V time scale is short compared to the time scale for electrical energy deposition in the gas.

The vibrational deactivation by V-T collision is expected to be very slow based on a theoretical extrapolation[3] from the measured deactivation rate constant of the first vibrational level. It is precisely this slow deactivation that permits the relatively efficient operation of the CO laser for long pulse lengths. Unfortunately there is no experimental confirmation of the predicted deactivation rate constants for the high vibrational levels. Furthermore, the practical laser performance may be extremely susceptible to the effect of impurities which can provide large deactivation cross sections.[6-8] There is some experimental confirmation of this effect[9, 10] and it should be pointed out that the very high efficiencies predicted by calculations such as those described in this report may only be achievable in high purity gas systems.

The electron impact excitation function can be written in the form

$$E_v = N_e \sum_i \left( k_e^{i,v} N_i - k_e^{v,i} N_v \right) \qquad \text{(A-4)}$$

where $N_e$ is the electron density and $k_e^{i,v}$ is the rate constant for electron impact excitation from level i to level v. This rate constant requires detailed knowledge of the plasma kinetics. For a uniform discharge with a constant ratio of electric field to gas density, E/N, one solves the Boltzman equation for the non-Maxwellian electron velocity distribution function which is then integrated over the vibrational excitation cross-section data to obtain the necessary excitation rate constants. The accuracy of this approach is dependent upon the accuracy and availability of the necessary excitation cross-section data.[11-13] The electron impact vibrational cross sections have been measured from zeroth to the first nine excited vibrational levels and such cross-section data have been used previously[14, 15] to calculate the electron velocity distribution function. The calculations indicate that the electrical energy is efficiently coupled to the vibrational mode at average electron temperatures of approximately 1 eV with a typical efficiency of over 98%. Recent calculations[16] suggest that the predicted rotational excitation, of the order of 1/2 to 1% of the discharge energy, may be underestimated by an order of magnitude. This would increase the rate of change in the translational temperature which is dominated by V-V vibrational relaxation in the present calculations, the energy defect in the V-V process being taken up in the translation/rotation modes.

Several approximations used in the earlier analyses have been made in the present discharge analysis. Collisions of the second kind were neglected in determining the electron velocity distribution function. Furthermore, electron impact excitation was neglected from any vibrational level other than the zeroth vibrational level. This simply reflects the lack of

theoretical and/or experimental data in CO. Discharge calculations[15] in $N_2$ have shown that the inclusion of excitation/deexcitation from excited levels leads to a different distribution in the excitation rate constant to the individual vibrational levels. However, the overall excitation rate, $\Sigma v k_v$, was found to be quite insensitive to the excited state distribution. Although these approximations lead to errors in the excitation rate constants they are not expected to have a major effect on the numerical calculations for high pressure electrical lasers. This conclusion follows from considerations of the operating conditions in these lasers, typically electron beam sustained discharges. The pressure is usually high enough so that the characteristic time scale for molecular relaxation processes, of the order of $10^{-6}$ to $10^{-7}$ secs, is much smaller than the corresponding time scale for vibrational excitation which is of the order of $10^{-3}$ to $10^{-5}$ secs. As a result, errors in the electron impact excitation rate constants to individual vibrational levels tend to get washed out in the vibrational kinetics and the net effect is a small error in the overall excitation rate, $\Sigma v k_v$, which is equivalent to a corresponding change in the electron density and which effect can be estimated from simple scaling considerations described below.

In the determination of the cavity flux it is assumed that the rotational levels are in thermal equilibrium with the translational temperature and that the rotational relaxation is fast enough so that only one rotational line is allowed to oscillate in any given vibrational transition. Furthermore, the cavity flux for each vibrational transition is assumed to be zero unless and until the small signal gain for that particular transition becomes equal to the appropriate cavity loss. After this the steady-state approximation, gain equals loss, is made and the stimulated emission/absorption term is described by

$$S_{v+1,\,v} = g_{v+1,\,v}\,\phi_{v+1,\,v}/h\nu_{v+1,\,v} \tag{A-5}$$

where $g_{v+1,\,v}$ is the saturated gain and $\phi_{v+1,\,v}$ is the cavity flux for the transition $v+1 \rightarrow v$ with frequency $\nu_{v+1,\,v}$. The small signal gain can be shown[17] to be given by an expression of the form

$$g_{\substack{v+1,\,v \\ J-1,\,J}} = K\,\nu_{v+1,\,v}\,J(v+1)\,\Theta_v\,e^{-J(J+1)\,\Theta_v/T} \left\{(1-\epsilon_v)\,N_{v+1}\,e^{2J\left(1+\frac{J-1}{2}\,\epsilon_v\right)\Theta_v/T} - N_v\right\} \tag{A-6}$$

where J refers to the particular rotational level, $\epsilon_v$ is a small anharmonic correction to the rotational constant, $\Theta_v$ is the characteristic vibrational temperature, and K is a function of the molecular constants together with the line broadening parameters. In the present case, for high pressure electrical discharges the transitions are pressure broadened. An inherent assumption in this analysis is the neglect of spatial variations in the cavity flux. It can be readily shown that the maximum axial variation in the

cavity flux is less than 10% for an output coupling, Lc, of 60% or less. For the present calculations the optical cavity is assumed to be formed by two mirrors of reflectivities $R_1$ (= 1 - $a_1$) and $R_2$ (= 1 - $a_2$ - Lc) with mirror losses of $a_1$ and $a_2$ respectively. Using the steady-state condition $R_1 R_2 \exp(2 g \ell) = 1$ it can be shown that the output flux is given by

$$\frac{\phi_{out}}{\phi} = \frac{g\ell \, he}{R_2\left(e^{g\ell} - 1\right)\left(1 + R_1 e^{g\ell}\right)} \qquad (A-7)$$

where $\phi$ is the calculated internal cavity flux and $\ell$ is the length of the active medium.

Some comment should be made regarding the expected scaling with gas pressure and electron density Since only binary collision processes are included in the kinetic model, this scaling is relatively simple. The master equation can be nondimensionalized by the use of particle densities which have been normalized by the total gas density, N. The collisional terms can then be written directly in terms of these normalized densities and the term containing the natural lifetime can be neglected in comparison with the V-V and stimulated emission terms. The electron density becomes normalized by the total gas density and the dimensionless stimulated emission term behaves like $\phi/N^2$ as a result of the small signal gain varying with total gas density and inversely with the pressure broadened linewidth. It follows then that for fixed ratio of electron density to total gas density, Ne/N, the flux should scale with the square of the gas density, $\phi \sim N^2$, and the time should scale inversely with gas density, $\tau \sim N^{-1}$. In this simple scaling relation the effect of temperature variations on the collisional rate constants and the line broadening have been neglected. The errors introduced by this approximation have been shown to be neglected by numerical calculations.

## APPENDIX A

## REFERENCES


1. Caledonia, G. E. and Center, R. E., J. Chem. Phys. 55, 552 (1971).

2. Smith, I. W. M. and Wittig, C., Faraday Transactions II, 7, 939 (1973).

3. Sackett, P. B., Hordvik, A. and Schlossberg, H., Appl. Phys. Lett. 22, 367 (1973).

4. Stephenson, J. C., Appl. Phys. Lett. 22, 576 (1973).

5. Powell, H. T., J. Chem. Phys. 59, 4937 (1973).

6. vonRosenberg, C. W., Jr. and Wray, K. L. and Teare, J. D., J. Chem. Phys. 54, 1974 (1971).

7. vonRosenberg, C. W., Jr. and Wray, K. L., J. Chem. Phys. 54, 1406 (1971).

8. Center, R. E., J. Chem. Phys. 58. 5230 (1973).

9. Boness, M. J. W. and Center, R. E., Avco Everett Research Laboratory Report "Carbon Monoxide Laser" Annual Technical Report, May 1974. Contract No. N00014-72-C-0030.

10. Mann, M. M., private communication.

11. Schulz, G. J., Rev. Mod. Phys. 45, 423 (1973).

12. Ehrhardt, H., Langhans, L. Linder, F. and Taylor, H. S., Phys. Rev. 173, 222 (1968).

13. Boness, M. J. W. and Schulz, G. J., Phys. Rev. A 8, 2883 (1973).

14. Hake, R. D. Jr. and Phelps, A. V., Phys, Rev. 158, 70 (1967).

15. Nighan, W. L., Appl. Phys. Lett. 20, 96 (1972).

16. Chandra, N. and Burke, P. G., J. Phys. B: Atom. Molec. Phys., 6, 2355 (1973).

17. Penner, S. S., Quantitative Molecular Spectroscopy and Gas Emissivities, Addison-Wesley, Reading. Mass. (1959).